IEEE Access
Multidisciplinary ⋮ Rapid Review ⋮ Open Access Journal

Received January 31, 2021, accepted February 15, 2021, date of publication February 23, 2021, date of current version March 4, 2021.

Digital Object Identifier 10.1109/ACCESS.2021.3061471

Surrogate-Assisted Multi-Objective Probabilistic Optimal Power Flow for Distribution Network With Photovoltaic Generation and Electric Vehicles

CHITCHAI SRITHAPON[1,2], (Graduate Student Member, IEEE), PRADIT FUANGFOO[2], PRASANTA K. GHOSH[3], (Life Senior Member, IEEE), APIRAT SIRITARATIWAT[1], AND RONGRIT CHATTHAWORN[1]

[1]Department of Electrical Engineering, Faculty of Engineering, Khon Kaen University, Khon Kaen 40002, Thailand
[2]Provincial Electricity Authority (PEA), Bangkok 41000, Thailand
[3]Department of Electrical Engineering and Computer Science, Syracuse University, Syracuse, NY 13244, USA

Corresponding author: Rongrit Chatthaworn (rongch@kku.ac.th)

This work was supported in part by the Faculty of Engineering, Khon Kaen University, under Grant Ph.D.Ee-1/2562, and in part by the National Research Council of Thailand under the program Research Grant for New Scholar.

ABSTRACT The uncertainties of solar photovoltaics generation, electric vehicle charging demand, and home appliances load are the major challenge of energy management planning in the residential areas. Optimal allocation of battery energy storage systems for distribution networks based on probabilistic power flow (PPF) is an effective solution to deal with these uncertainties. However, the high computational burden is the main obstacle of this method. Therefore, this paper proposes a surrogate-assisted multi-objective probabilistic optimal power flow (POPF) to reduce the expensive computational time. The surrogate model is developed by using a machine learning method namely deep learning which is used for bypassing the deterministic load flow calculation. Zhao's point estimation method combined with Nataf transformation is selected to handle the PPF analysis considering correlated uncertain input variables. The multi-objective POPF problem is solved using the multi-objective differential evolution. The historical data including solar irradiation, ambient temperature, residential load, and electric vehicle (EV) travel distance is calculated in the low voltage distribution system to demonstrate the potential advantages of the proposed method. Numerical results show that the proposed surrogate assisted multi-objective POPF method provides the optimal solution for operating cost, helps to prolong transformer life and reducing environmental impact. Moreover, the results show that the proposed surrogate-assisted optimization framework gives a better solution when comparing with the conventional surrogate-assisted method.

INDEX TERMS Battery energy storage system, carbon emission, deep learning, multi-objective differential evolution, probabilistic power flow, transformer loss of life, Zhao's point estimation method.

I. INTRODUCTION

Climate change and global warming problems due to the greenhouse effect are damaging the world we live in. To save the environment, greenhouse gas emissions of CO_2 must be reduced. One realistic way to reduce CO_2 emission is to increase the power generation from renewable energy sources (RES). In the present day, the installation costs of solar photovoltaic (PV) systems are continuously going down and electricity prices from solar PV will be shortly reasonable for residential usage [1]. Besides, electric vehicle (EV) is becoming the new paradigm of transportation for reducing carbon emissions [2]. Therefore, many governments are promoting the use of solar PV and EVs [3].

Increased solar PV systems can impact power networks, especially on low voltage distribution networks. These negative impacts include power quality issues, such as power fluctuation due to solar irradiation variation and overvoltage conditions when solar PV generation exceeding the demand. Moreover, the stochastic behavior of EV traveling, vehicle

The associate editor coordinating the review of this manuscript and approving it for publication was Li Zhang.

model, and charger equipment also increase uncertainty in the existing power system.

Several researchers studied ways to mitigate the negative impacts of RES integration in the network. Research works of Yang *et al.* [4], May *et al.* [5], and Hesse *et al.* [6] proposed the use of an energy storage system (ESS) because its technology and price will be reasonable for utility and residential applications in the near future. Barai *et al.* [7] proposed optimal use of ESS for flattening the power demand curve. In references, [8]–[10] authors presented the optimal ESS for economical optimal power flow in the power system with integrated RES. Also, authors in [11] proposed a method of day-ahead and real-time optimal power flow (OPF) that considers the security and variability cost of RESs. However, all the above-mentioned works have not considered the impact of the uncertainty in the optimization problem.

The power generation by the RES varies with the environment. For example, solar PV output power varies with solar radiation and temperature while wind turbine (WT) power output depends on the wind speed. Additionally, solar irradiance, wind speed, and ambient temperature are highly uncertain because of geographic location, seasons of the year, as well as atmospheric condition and climate at that time. There are papers on the study of POPF in uncertain environments. For instance, the probabilistic optimal battery size and operation in the power system was presented in [12]–[14]. Authors in reference [15] have proposed the optimal energy storage allocation for mitigating the unbalance in the distribution network using the Rosenblatt transformation to quantify the probabilistic voltage unbalance factor. The probabilistic method is the appropriate tool for power flow calculation from the point of view of the uncertainties. The probabilistic power flow (PPF) uses the probability density functions (PDF) to represent the uncertainty of input parameters then obtains the PDF of output variables to characterize their uncertainty. Generally, the PPF process consists of three main steps [16]. The first step is the modeling of the input uncertainty based on the obtained PDF. Next is the computation of PPF. The final step is analyzing the PDF of the output variable. Typically, Monte Carlo simulation (MCS), convolution method, cumulant method, and point estimate method (PEM) are often used in the PPF computation.

The MCS is the numerical method often being used to compute the PPF. The deterministic load flow (DLF) calculations are repeatedly performed using samples from the input PDF to generate the output probability distributions. There are some studies on the POPF using the MCS [17], [18]. To improve the accuracy of the PPF output results, a large number of samples is required which in turn leads to an expensive computational burden. Therefore, the MCS has commonly been used as the benchmark for comparison and validation of the proposed PPF method [16], [19]. The PPF calculation using the convolution method is the analytic method. This method uses a linear mathematical function of the power flow equations with moments of the PDF to estimate the PPF results [20], [21]. However, this also needs significant computation time for convolution calculation and consequently rarely deployed for the POPF in recent studies.

The cumulant method (CM) approach has been introduced to relieve the computational burden from the convolution calculation. This PPF method uses the cumulants of the input PDF to evaluate the cumulants of the output PDF [22], [23]. However, the CM cannot handle the PPF analysis considering the correlation of input variables. On the other hand, the PEM is the approximation method for solving the PPF problem. This method selects the m appropriate estimating points with their corresponding weight coefficients to represent the distribution of each input variable. Then the PDF and an expected value of the interesting output variables are estimated by taking every sample point of all the considered input variables. Normally, using the PEM by default is not suitable for dealing with the correlated variables. Hence, a multivariate transformation such as the Rosenblatt transformation and Nataf transformation is commonly used in combination with PEM to handle the correlation between uncertain input variables [24], [25]. Authors in [26] presented a multi-objective POPF for sizing and siting of PVs, WTs, and capacitor banks in the power system using the PEM combined Nataf transformation to deal with the correlated random inputs variables. A new probabilistic model based on Gaussian and Archimedean copulas for modeling the uncertainty and variability of wind power generation is proposed in [27]. However, it can be observed that most of the PPFs still require to perform a deterministic load flow calculation in the process. Hence, the above POPF for energy system planning needs a long computing time, especially in the context of considering many uncertainty input variables.

Nowadays, Nowadays, surrogate models are used in various areas of engineering fields to reduce expensive computational time. The surrogate model is used to approximate output from input data based on the behavior of complex systems without the mathematically extensive models. For example, authors in [28] introduced the basis-adaptive sparse polynomial chaos expansion (SPCE) as the surrogate model to perform the PPF analysis in the power systems. The SPCE method is also used to obtain the probabilistic models for microgrid load margins in [29]. The surrogate-assisted optimization for the aerodynamic design of an aircraft wing is presented in [30]. Researchers in [31] proposed the surrogate-assisted robust optimization for the photovoltaic-electrolyzer system design under uncertainties. Machine learning based on supervised learning such as support vector machines (SVM) and artificial neural networks (ANN) is often used to construct the surrogate model [32]–[34]. Specifically, in [35], the ANN surrogate model is used to represent an actual engineering model (AEM) of the energy system in the optimization process and showed that can reduce the computational time by 84%. However, it can be observed that the output of the surrogate model can deviate from the actual model. Hence, most of the surrogate-assisted optimization frameworks still need to run the algorithm using the AEM as one of the

steps. This can lead to an increase in the computation time of the conventional surrogate-assisted optimization method. Therefore, to overcome the above limitations in the previous studies, this paper proposes a new surrogate-assisted multi-objective POPF method for the distribution network with solar PVs and EVs considering the correlation of the uncertainty input variables. The main contributions of this study can be summarized as follows:

- This paper introduces the machine learning method namely deep learning to develop a surrogate model for distribution networks with integrated solar PVs and EVs. The deep learning module in an open-source Python library can be simply used to construct the surrogate model which provides high accuracy.
- The proposed novel surrogate-assisted multi-objective POPF method reduces the computational burden.
- The study of the best trade-off solution between three objective functions consisting of economic cost, transformer loss of life, and carbon emission for the optimal Battery Energy Storage System (BESS) allocation in the power system is demonstrated for the first time in this research.

The paper is organized as follows: Section II presents the probabilistic power flow method adopted in this study, and in Section III, the problem formulation is explained. The proposed methodology in this work is described in Section IV. Section V illustrates the simulation results followed by a discussion in Section VI. Finally, conclusions are given in Section VII.

II. PROBABILISTIC POWER FLOW

In this section, the stochastic models of residential load, PV power generation, and EV charging demand in the distribution network are described in the first subsection. Then, a competitive probabilistic power flow analysis method, i.e., the point estimation method (PEM) combined with the Nataf transformation is explained in the next subsection.

A. UNCERTAINTY MODELING

The most important step of the PPF evaluation is to formulate an appropriate model for the uncertainties in the power system. In this work, the renewable source taken into account is only solar PV. Therefore, only solar irradiance and ambient temperature are considered in the presented uncertainty model of solar PV. In the power demand uncertainty model, we have considered two input variables including the conventional baseload, and EV charging demand. Normally, the uncertain characteristic of these variables depends according to times of day, seasons of the year, and the energy price rate.

1) LOAD AND TEMPERATURE MODEL

The uncertainties of residential load and ambient temperature are commonly modeled using a normal probability density function (PDF) [36]–[38]. The general normal PDF can be written as follows:

$$f(x) = \frac{1}{\sigma\sqrt{2\pi}} \exp(-\frac{(x-\mu)^2}{2\sigma^2}) \tag{1}$$

where x is the studied variable which is either load or the ambient temperature. μ and σ are the mean and the standard deviation of its distribution, respectively. In this paper, only the active load power (kW) is modeled as a random variable while the reactive power varies with the active power based on a power factor of the load model.

2) PV POWER GENERATION

PV power production depends directly on the number of installing arrays, cell specifications, solar irradiation, and ambient temperature [20]. Thus, the PV power generation uncertainty model can be introduced as a PDF of the solar irradiance and environment temperature. The stochastic model of solar irradiation is usually modeled by beta distribution [32], [39] while the normal distribution is typically used for modeling the uncertain ambient temperature [40], [41]. The general beta PDF of solar irradiation can be modeled as follows:

$$f(r) = \frac{\Gamma(\alpha+\beta)}{\Gamma(\alpha)+\Gamma(\beta)} r^{\alpha-1}(1-r)\beta \tag{2}$$

where r is the solar radiation (W/m^2). α and β denote as the exponents of the random variable and control variable for the distribution shape, respectively. Γ is the gamma function.

Based on the above-mentioned distribution functions of solar irradiation and environment temperature, the stochastic model of PV output power can be formulated by the following equations [32]:

$$P_{PV,t} = \eta_{PV} PV_r R_t [1 + \alpha_P (T_{C,t} - T_{C,STC})] \tag{3}$$

$$T_{C,t} = T_{a,t} + R_t (NOCT - 20) \tag{4}$$

where

$$R_t = \begin{cases} \frac{r_t^2}{r_c r_{std}} & r_t < r_c \\ \frac{r_t}{r_{std}} & r_c \le r_t \le r_{std} \\ r_{std} & r_t > r_{std} \end{cases} \tag{5}$$

$P_{PV,t}$ denotes PV output power (kW) at time t, PV_r is the power rating of PV module (kW) and η_{PV} is the overall PV system efficiency including converter components. α_P is the power temperature coefficient (W/°C). $T_{C,t}$ and $T_{a,t}$ are PV cell temperature (°C) and ambient temperature (°C) at time t, respectively. $T_{C,STC}$ is a reference cell temperature under standard test conditions (STC). $NOCT$ is the nominal operating cell temperature (°C). r_t is the global solar irradiation (W/m^2) at time t. r_{std} is the solar radiation under STC, which is normally set to 1,000 W/m^2 and r_c is a certain radiation point, typically set as 150 W/m^2.

3) EV CHARGING DEMAND

The stochastic model of EV charging demand in the residence is usually evaluated based on the probability distribution of

arrival time, departure time, daily travel distance, and type of vehicle. Based on the survey data from National Household Travel Survey (NHTS) [42], the uncertainties of the arrival and departure time can be modeled using the normal PDF while the daily travel distance is usually modeled using the lognormal distribution. The lognormal PDF can be expressed by the following equation [43]:

$$f(d) = \frac{1}{d\sigma\sqrt{2\pi}} \exp\left[-\frac{(\ln d - \mu)^2}{2\sigma^2}\right] \tag{6}$$

Moreover, electricity tariffs such as the time of use (TOU) rate can motivate EV owners to charge their EVs at a lower price period. Hence, to generate the stochastic model of EV charging demand, the electricity price rate should be taken into account. The following steps are performed using the MCS method to evaluate the PDF of hourly EV charging demand in the distribution network considering the effect of the TOU rate.

Step 1: Referring to the study in [44], [45], the probability of expected EVs charging start time (T_{st}) to account for the effect of the TOU rate is described below [45]:

$$C(t) = \begin{cases} c_{off-peak} & 1 \le t < 9, 22 \le t \le 24 \\ c_{peak} & 9 \le t < 22 \end{cases} \tag{7}$$

$$P(t) = \begin{cases} 1\% & 2 \le t < 19 \\ 6\% & 19 \le t < 22 \\ 15\% & 1 \le t < 2, 22 \le t \le 24 \end{cases} \tag{8}$$

where $C(t)$ is the TOU tariff function and c_{peak} and $c_{off-peak}$ are the electricity prices at peak time and off-peak time, respectively. $P(t)$ is the probability of the expected EVs to start charging at hour t. Next, the number of EVs that start charging at hour t can be determined as follows:

$$n_{ev,t} = P(t)N_{EV} \tag{9}$$

where $n_{ev,t}$ denotes the number of EVs that start charging at hour t while N_{EV} is the total number of EVs under study.

Step 2: In this paper, we assume all EV owners would like to charge their vehicle closed to full charge as much as possible at home. Therefore, the required charging duration (T_{ch}) of each EV can be calculated using the following equation:

$$T_{ch} = \varepsilon d / \eta_{EV} P_{ch} \tag{10}$$

where ε is the electricity consumption rate of EV (kWh/km) which depends on the type of EV model. d is the randomized daily travel distance (km). P_{ch} and η_{EV} are EV charger power rating (kW) and EV charging efficiency, respectively.

Step 3: According to the charging start time ($T_{st,i}$) in step 1 and the charging duration in step 2, the hourly charging of the i^{th} EV ($H_{ch,i}$) can be determined as follows:

$$H_{ch,i} = T_{st,t} + k \quad \text{for} \quad k = 0, 1, 2, \ldots, T_{ch} - 1 \tag{11}$$

Step 4: Finally, the hourly probability of EV charging is evaluated using the MCS method. The algorithm to evaluate the stochastic model of hourly EV charging demand in the distribution network is presented in Fig. 1.

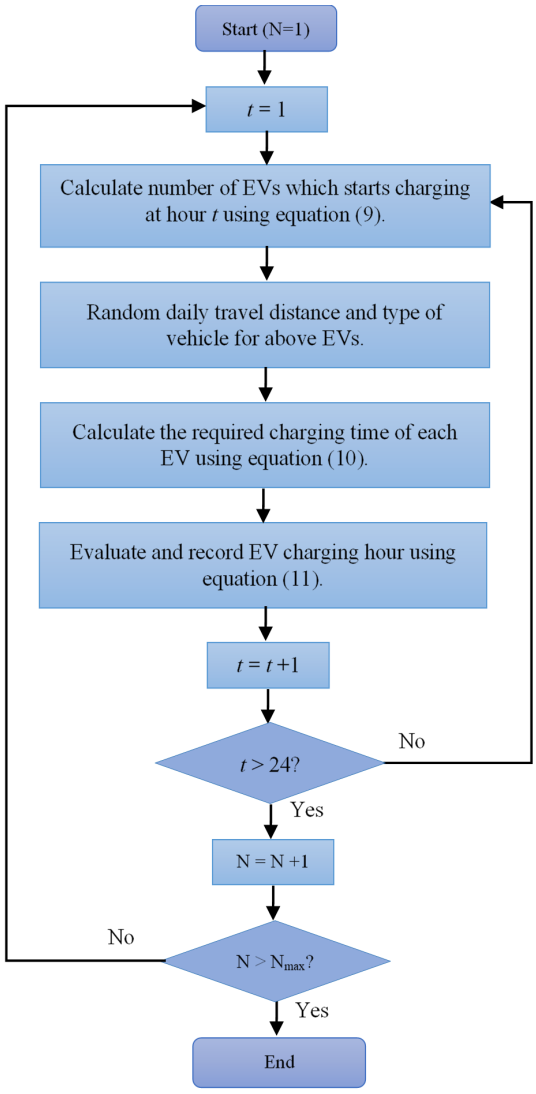

FIGURE 1. Algorithm for generation of hourly stochastic of EV charging.

From the flowchart in Fig. 1, the algorithm begins by setting iteration (N) and t equal to 1. The number of EVs that start charging at the hour t is determined using equation (9) and considering the probability function as shown in equation (8). Then the daily travel distance and the type of vehicle model of each EV are randomly generated using the lognormal distribution and the proportional distribution, respectively. Next, the required charging time is calculated using equation (10) and then evaluation and recording of the hourly charging are done for all EVs using equation (11). This MCS process will continue until the time reaches the 24th hour for each iteration. After that, the algorithm will be repeated in the next iteration and will stop when the number of iteration (N) reaches the maximum iteration (N_{max}).

B. PEM COMBINED WITH NATAF TRANSFORMATION

PEM is the efficient PPF analysis method when considering the balance between accuracy and computation burden.

Therefore, this paper selects the PEM for decreasing the calculation time for the PPF evaluation while it still maintains the appropriate level of accuracy. Also, several studies presented that the PPF analysis using Zhao's PEM is more accurate than Hong's PEM [46], [47]. Additionally, according to the study in reference [19] and [48], the Nataf transformation shows more practical deployment than the Rosenblatt transformation when dealing with the correlated non-normal input variables. Hence, in this study, the Nataf transformation is chosen to be used with Zhao's PEM for handling the correlation of the input variables.

1) NATAF TRANSFORMATION

The Nataf transformation maps the correlated random samples from the original distribution space to the standard Gaussian space [49]. Hence, we use Nataf transformation to generate the correlated input variable samples in the original distribution based on the selected samples in the standard normal distribution space as follows:

$$\begin{pmatrix} u_1 \\ \vdots \\ u_i \\ \vdots \\ u_m \end{pmatrix} \begin{matrix} R_z = LL^T \\ \downarrow \\ Z = LU \\ \rightarrow \end{matrix} \begin{pmatrix} z_1 \\ \vdots \\ z_i \\ \vdots \\ z_m \end{pmatrix} \begin{matrix} \\ \\ x_i = F^{-1}[\phi(z_i)] \\ \rightarrow \end{matrix} \begin{pmatrix} x_1 \\ \vdots \\ x_i \\ \vdots \\ x_m \end{pmatrix} \tag{12}$$

where

$$Rz = \begin{bmatrix} \rho_{z,11} & \rho_{z,12} & \cdots & \rho_{z,1n} \\ \rho_{z,21} & \rho_{z,22} & \cdots & \rho_{z,2n} \\ \vdots & \vdots & \ddots & \vdots \\ \rho_{z,n1} & \rho_{z,n2} & \cdots & \rho_{z,nn} \end{bmatrix} \tag{13}$$

$$Rx = \begin{bmatrix} \rho_{x,11} & \rho_{x,12} & \cdots & \rho_{x,1n} \\ \rho_{x,21} & \rho_{x,22} & \cdots & \rho_{x,2n} \\ \vdots & \vdots & \ddots & \vdots \\ \rho_{x,n1} & \rho_{x,n2} & \cdots & \rho_{x,nn} \end{bmatrix} \tag{14}$$

Suppose Rx is a correlation matrix of random vectors X in the original space. $\rho_{x,ij}$ is a correlation coefficient between i^{th} and j^{th} input variables which is obtained by using Spearman's rank-order correlation method [50]. The correlation coefficient component of matrix R_Z can be determined as $\rho_{z,ij} = T\rho_{x,ij}$. The approximate expressions of T are based on the polynomial function of the variation of marginal distribution, more explanation of function T can be found in [49]. Besides, $U = [u_1, \ldots, u_i, \ldots, u_m]^T$ is an independent standard normal vector and $Z = [z_1, \ldots, z_i, \ldots, z_m]^T$, is a correlated vector in the standard Gaussian distribution space. L represents the lower triangular matrix from Cholesky decomposition and denotes as $Rz = LL^T$. Finally, the mapping from z to x expresses as $x_i = F^{-1}[\phi(z_i)]$ where $\phi(z_i)$ is the cumulative distribution function (CDF) of the standard normal variable z_i while $F^{-1}(\cdot)$ is the inverse CDF of x_i.

2) ZHAO'S PEM

Zhao's PEM with a five-point estimation is proposed to evaluate the PPF problem in this paper. The typically selected points together with their corresponding weight coefficients can be determined using Gaussian–Hermite integration and can be found in [46]. A matrix of n input variables at the k^{th} estimating point can be written as follows:

$$X_k = \begin{bmatrix} x_{1,k} & \mu_{x2} & \cdots & \mu_{xn} \\ \mu_{x1} & x_{1,k} & \cdots & \mu_{xn} \\ \vdots & \vdots & \ddots & \vdots \\ \mu_{x1} & \mu_{x2} & \cdots & x_{n,k} \end{bmatrix} \tag{15}$$

where $x_{i,k}$ and μ_{xi} are the k^{th} estimating point and mean of the i^{th} input variable, respectively. In this context, $k = 1, 2 \ldots, m$ and $i = 1, 2 \ldots, n$.

Next, each row of matrix X_k is used as input variables for a deterministic load flow (DLF) calculation. The process continues for all pending rows and the remaining input matrices. It should be noted that the matrix of the estimating point at mean required only one DLF computing round because all rows include the same components with the mean value of the input variables. Hence, Zhao's PEM needs to calculate the DLF with $(m-1)n+1$ times. Lastly, an expected value (y), mean (μ_y) and standard deviation (σ_y) of the PPF output variable can be evaluated using the following expression [46]:

$$y \approx g_\mu + \sum_{i=1}^{n} (g_i - g_\mu) \tag{16}$$

$$\mu_y = g_\mu + \sum_{i=1}^{n} (\mu_i - g_\mu) \tag{17}$$

$$\sigma_y = \sqrt{\sum_{i=1}^{n} \sigma_i^2} \tag{18}$$

where

$$g_i = g[N^{-1}(U_i)] \tag{19}$$

$$\mu_i = \sum_{k=1}^{m} w_k g[N^{-1}(u_{i,k})] \tag{20}$$

$$\sigma_i^2 = \sum_{k=1}^{m} w_k (g[N^{-1}(u_{i,k})] - \mu_i)^2 \tag{21}$$

Here, g_i means the DLF computation with U_i which is taken as the estimated point while the other variables are fixed at the mean point. Besides, g_μ is the DLF calculation result when all input variables are set equal to mean values. $N^{-1}(\cdot)$ is the inverse Nataf transformation. $u_{i,k}$ and w_k are the Gaussian quadrature node and its coefficient weight, respectively.

III. PROBLEM FORMULATION

In this paper, the optimal BESS allocation for the POPF in the distribution network with PVs and EVs is proposed. The decision variable for optimized BESS is determined based on the PPF analysis subject to the optimization constraints.

A. OBJECTIVE FUNCTIONS

The objective functions of a probabilistic multi-objective OPF consist of economic cost, transformer aging, and carbon emission. Formulations of three objective functions are described as follows.

1) ECONOMIC COST

The economic cost is formulated as an annual cost which includes electricity cost and BESS deployment cost. The electricity cost is calculated for 3 seasons of a year consisting of winter, summer, and rainy. The cost of battery implementation consists of capital cost ($BESS_{cap}$) and operation and maintenance costs ($BESS_{o\&m}$). The economic cost function can then be presented as follows:

$$\min f_1 = \sum_{s=1}^{3}\left(Nd_s\sum_{t=1}^{24}\left(Pg_{s,t}Cg_t + Ppv_{s,t}Cpv_t\right)\right) + BESS_{cap} + BESS_{o\&m} \quad (22)$$

$$BESS_{cap} = C(r,y)\cdot\left(Cp_{cap}Pb_r + Ce_{cap}Eb_r\right) \quad (23)$$

$$BESS_{o\&m} = Cp_{o\&m}Pb_r + Ce_{o\&m}Eb_r \quad (24)$$

$$C(r,y) = \frac{r(1+r)^y}{(1+r)^y - 1} \quad (25)$$

where $Pg_{s,t}$ and $Ppv_{s,t}$ are the imported power (kW) from the main grid and the surplus power from the PV systems at hour t in season s^{th}, respectively. Cg_t and Cpv_t are electricity prices (\$/kWh) of energy purchased from the grid and PV systems at time t, respectively. Nd_s is the total number of days in each season. Pb_r and Eb_r are battery power rating (kW) and energy capacity rating (kWh), respectively. Besides, $C(r,y)$ represents the capital recovery factor which is used to calculate the present value of an annual cost. r and y are the interest rate and the project lifetime in years.

2) TRANSFORMER LOSS OF LIFE

The transformer loss of life is taken as the technical objective in this study. According to the IEEE standard C57.91 [51], the transformer aging is mostly estimated from the transformer insulation life. The objective function of an annual transformer loss of life can be written as follows:

$$\min f_2 = \sum_{s=1}^{3} Nd_s \sum_{t=1}^{24} F_{s,t}^{AA}\Delta t \quad (26)$$

where F_t^{AA} is the aging acceleration factor of season s^{th} at hour t and its value relates to a winding hottest-spot temperature (θ_t^H). This factor can be evaluated using the following expressions:

$$F_t^{AA} = \exp\left[\frac{15000}{383} - \frac{15000}{\theta_t^H + 273}\right] \quad (27)$$

$$\theta_t^H = \theta_t^A + \Delta\theta_t^{To} + \Delta\theta_t^H \quad (28)$$

where θ_t^A is the ambient temperature at the time t while $\Delta\theta_t^{To}$ and $\Delta\theta_t^H$ are top-oil temperature rise over the ambient temperature and winding hottest-spot temperature rise over the top-oil temperature at the end of time t, respectively. It should be noted that all variables are in degrees Celsius (°C).

The expressions of $\Delta\theta_t^{To}$ and $\Delta\theta_t^H$ are given by the exponential function containing a temperature-time constant as follows [52]:

$$\Delta\theta_t^{To} = (\Delta\theta_t^{To,U} - \Delta\theta_{t-1}^{To})(1 - e^{-\Delta t/\tau_o}) + \Delta\theta_{t-1}^{To} \quad (29)$$

$$\Delta\theta_t^{H} = (\Delta\theta_t^{H,U} - \Delta\theta_{t-1}^{H})(1 - e^{-\Delta t/\tau_w}) + \Delta\theta_{t-1}^{H} \quad (30)$$

where $\Delta\theta_t^{To,U}$ and $\Delta\theta_{t-1}^{To}$ are the highest top-oil temperature at time t and a previous state, respectively. $\Delta\theta_t^{H,U}$ and $\Delta\theta_{t-1}^{H}$ are the maximum winding hottest-spot temperature at the time t and at the previous time, respectively. Also, τ_o and τ_w are the time constant of oil and winding, respectively. The value of $\Delta\theta_t^{To,U}$ and $\Delta\theta_t^{H,U}$ depend on transformer specification and its loading which can be expressed in the following equations:

$$\Delta\theta_t^{To,U} = \Delta\theta_r^{To}\left[\frac{k_t^2R + 1}{R+1}\right]^n \quad (31)$$

$$\Delta\theta_t^{H,U} = \Delta\theta_r^{H}k_t^{2m} \quad (32)$$

where $\Delta\theta_r^{To}$ and $\Delta\theta_r^{H}$ are the ultimate temperature rise of the top-oil and winding hottest-spot when the transformer is operating at its rated power, respectively. k_t is the ratio of transformer loading and its power rating at time t. R is the ratio of transformer power loss at full load rating and no-load. In addition, m and n are an empirically cooling exponent parameter of transformer winding and oil, respectively.

3) CARBON EMISSION

In this paper, the carbon emission is formulated as a function of the probabilistic power imported from the main grid with a mean carbon emission rate (Cc_{emis}) at any hour. The emission is calculated for a year. The objective function can then be defined as follows:

$$\min f_3 = \sum_{s=1}^{3} Nd_s \sum_{t=1}^{24} Pg_{s,t}Cc_{emis} \quad (33)$$

Finally, the general expression of multi-objective POPF with correlated input variables can be formulated as shown below.

$$F_{POPF} = \min\{f_1(X,Y), f_2(X,Y), f_3(X,Y)\} \quad (34)$$

where F_{POPF} is the multi-objective POPF function. X is the set of control decision variables, which here is the battery power dispatching at any time. Y is the vector of uncertain input variables of the PPF problem such as residential baseload, solar irradiation, ambient temperature, and EV charging demand.

B. CONSTRAINTS

All the above-mentioned objective functions should be optimized subject to the following constraints.

1) POWER BALANCE EQUATION

The constraints of active and reactive power balance equations in the power system are generally denoted as follows:

$$P_{G,i} - P_{L,i} = \sum_{j=1}^{Nb} V_iV_j\left(G_{ij}\cos\delta_{ij} + B_{ij}\sin\delta_{ij}\right) \quad (35)$$

$$Q_{G,i} - Q_{L,i} = \sum_{j=1}^{Nb} V_iV_j\left(G_{ij}\sin\delta_{ij} + B_{ij}\cos\delta_{ij}\right) \quad (36)$$

where $P_{G,i}$ and $P_{L,i}$ are active power generation and load at the i^{th} bus, respectively. Besides, $Q_{G,i}$ and $Q_{L,i}$ are reactive power generation and load at the i^{th} bus, respectively.

Note that the active power at each bus can be injected by the PV system or the BESS discharging power while the power demand consists of baseload, EV charging demand, and BESS charging power. V_i and V_j are voltage magnitude at the i^{th} and j^{th} buses, respectively. Also, $\delta_{ij} = \delta_i - \delta_j$, is the difference of angle between bus i and bus j voltage. N_b is the total number of power system buses. G_{ij} and B_{ij} are the real and imaginary parts of the component ij in the bus admittance matrix, respectively.

2) BATTERY CONSTRAINTS

To prolong the battery lifetime, daily charging and discharging energy should be balanced and its state of charge (SoC) must not exceed the limit level. These constraints can be expressed as follows:

$$\sum_{t=1}^{24} (\eta_{b,c} Pb_{c,t} - \frac{Pb_{d,t}}{\eta_{b,d}}) = 0 \tag{37}$$

$$SoC_{\min} \leq SoC_t \leq SoC_{\max} \tag{38}$$

where

$$SoC_t = (1-\gamma) SoC_{t-1} + \left(\eta_{b,c} Pb_{c,t} - \frac{Pb_{d,t}}{\eta_{b,d}}\right) / C_{bat} \tag{39}$$

$Pb_{c,t}$ and $Pb_{d,t}$ are battery charging and discharging powers (kW) at hour t, respectively. $\eta_{b,c}$ and $\eta_{d,c}$ are battery charging and discharging efficiencies, respectively. SoC_t and SoC_{t-1} are battery energy levels at time t and the previous state, respectively. SoC_{min} and SoC_{max} are the minimum and maximum limits of battery energy level, respectively. Also, γ denotes a self-discharge coefficient while C_{bat} is the battery energy capacity (kWh).

3) SECURITY CONSTRAINTS

Regarding the stochastic in the power flow manner, the distribution network operation stability should be kept in high confidence. That means the uncertain variables such as bus voltage, branch power, line current, and the transformer winding hottest-spot temperature should be within the safe operating limits at a high probability. Therefore, the chance-constrained approach method is suitable to deal with the probabilistic constrained problem. The network security operating chance constraints can be defined as follows:

$$\Pr\left\{V_{i,\min} \leq V_i \leq V_{i,\max}\right\} \geq \gamma_V \quad \forall i \in \psi_{bus} \tag{40}$$

$$\Pr\left\{S_k \leq S_{k,\max}\right\} \geq \gamma_S \quad \forall k \in \psi_{branch} \tag{41}$$

$$\Pr\left\{|I_l| \leq I_{l,\max}\right\} \geq \gamma_I \quad \forall l \in \psi_{line} \tag{42}$$

$$\Pr\{HST_x \leq HST_{\max}\} \geq \gamma_{HST} \quad \forall t \in \psi_{Tr} \tag{43}$$

where Pr{.} denotes as the probability of the constraints function. V_i represents the voltage of the i^{th} bus while $V_{i,min}$ and $V_{i,max}$ are minimum and maximum limits of voltage at the bus i, respectively. S_k is the apparent power (kVA) of the k^{th} branch and $S_{k,max}$ is its maximum apparent power limit. I_l and $I_{l,max}$ are the current (A) in the l^{th} conductor and its maximum value, respectively. HST_x and HST_{max} are the winding hottest-spot temperature of the x^{th} transformer and its maximum rated value, respectively. Ψ_{bus}, Ψ_{branch}, Ψ_{line} and Ψ_{Tr} are the set of buses, branches, conductor lines, and transformers in the power system, respectively. Finally, γ_V, γ_S, γ_I and γ_{HST} are the security confidence of bus voltage, branch power, line current, and the transformer winding hottest-spot temperature, respectively.

C. BATTERY OPTIMAL ALLOCATION STRATEGY

In this section, the proposed optimal strategy for BESS deployment to achieve the above-mentioned objectives is described. Firstly, the battery location for minimizing network power loss is identified. Next, daily power dispatching patterns of the BESS are determined. Finally, the sizing of the BESS is obtained from its maximum operating point.

1) LOCATION

Because the residential network is a small-scale network consisting of one or two feeders, the strategy for solving the optimal location of BESS focuses only on a single installation that will be more economical for investment. Refer to the study in [22], the center of gravity (COG) theory is an effective method to identify a BESS location for minimizing power loss. Therefore, the COG method is also applied to use in this work. More about how to determine the optimal placement using the COG method can be found in [53].

2) OPERATION AND SIZING

After performing the probabilistic load flow calculation on the residential network, baseload power at the substation with no BESS is obtained. Accordingly, the hourly battery power dispatching can be constructed using the load following control method (LFC) as expressed below:

$$Pb_{s,t} = \begin{cases} Pbase_{s,t} & Pbase_{s,t} < 0 \\ Pbase_{s,t} - P_{th,s} & Pbase_{s,t} > P_{th,s} \\ 0 & 0 \leq Pbase_{s,t} \leq P_{th,s} \end{cases} \tag{44}$$

where $Pb_{s,t}$ is the battery dispatching power at hour t in season s. When $Pb_{s,t}$ is a negative value, BESS operates in charging mode, and a positive value is discharging operation; otherwise, in idle. $Pbase_{s,t}$ is the baseload power of the transformer at hour t in season s. Also, $P_{th,s}$ is the decision variable of the discharging thresholds in each season and can be obtained from the optimization algorithm method. It should be noted that because the reactive power demand in the residential is usually small. Hence, in this paper, the battery dispatches only the active power. Finally, the power rating (Pb_r) and energy capacity rating (Eb_r) of BESS are calculated as follows:

$$Pb_r = \max\left(\left|Pb_{s,t}\right|\right) \quad \text{for } s = 1, 2, 3 \text{ and } t = 1, 2 \ldots, 24 \tag{45}$$

$$Eb_r = \max\left(\left|Eb_{s,t}\right|\right) / D \quad \text{for } s = 1, 2, 3 \text{ and } t = 1, 2 \ldots, 24 \tag{46}$$

where $\max\left(\left|Pb_{s,t}\right|\right)$ is the maximum battery dispatching power while $\max\left(\left|Eb_{s,t}\right|\right)$ is the maximum battery stored

energy. D is a depth range of battery operation between the highest and the lowest allowable battery SoC.

IV. METHODOLOGY

The energy optimization planning in the power system is usually conducted based on a numerical simulation. Also, the optimal power flow considering the stochastic model of the input variables is commonly computed based on the PPF method which in turn needs to perform the DLF. Hence, optimizing hourly dispatching through the time series usually consumes high computational time and may reach up to several days. However, this computational cost can be reduced by using the surrogate model.

A. SURROGATE MODEL

1) DEEP LEARNING

In recent years, the evolution of the artificial neural network (ANN) trends to be widely used in a lot of research areas. ANN has multiple hidden layers to automatically learn the raw input features, which overcomes the time-consuming steps in the traditional machine learning algorithms. Deep learning is part of machine learning families based on ANN architecture, such as deep neural networks (DNNs), recurrent neural networks (RNNs), and convolution neural networks (CNNs). Their layers consist of artificial neurons, inside neuron has weights for each input, a bias coefficient, and an activation function. Deep learning based on DNN architecture is often used to construct the surrogate model [54]–[56]. Accordingly, it is selected to use for the development of the surrogate model used in this study. An example of basic DNN architecture is shown in Fig. 2. This network could learn approximately two output functions from three input variables. It consists of two hidden processing layers in which each layer contains four neurons.

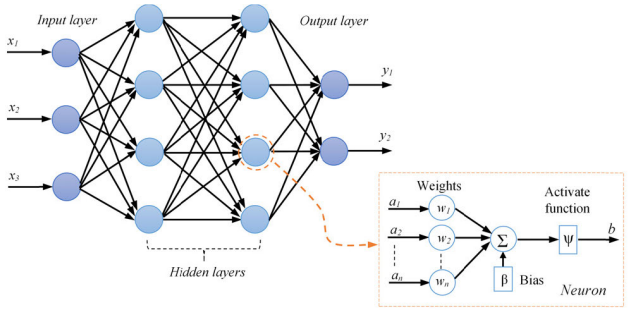

FIGURE 2. Example of a deep neural network (DNN).

2) DATASET GENERATION

PowerFactory DIgSILENT (PowerFactory) is the power system analysis software that is a convenient tool for load flow calculation [57], [58]. Using its load flow analysis package with the enhanced non-decoupled Newton-Raphson solution technique to solve the unbalanced load flow problem, can yields accurate results. Thus, the PowerFactory is selected to construct the actual engineering model (AEM) which is used to create a training dataset. Three steps to prepare the training dataset are described below:

Step 1) Construct the AEM of the power system using the PowerFactory in which each bus consists of a house baseload, a PV module and EVs. Also, the selected bus for BESS installation could be included with a battery model. Besides, the substation transformer is connected to the slack bus.

Step 2) Set a design of the experiment for simulation using the Latin hypercube sampling (LHS) method [59]. The input data of each hour such as baseload, solar irradiation, temperature and EV charging demand are uniform-randomly generated with a range of boundaries relate to their historical data while the battery dispatch power range is set based on the minimum and maximum value of power at the slack bus.

Step 3) Run load flow calculation with the experimental dataset and then collects the interesting output variables such as branch powers, grid power loss, bus voltages and line currents. In this paper, each hour has 5,000 samples that mean 120,000 samples are obtained in 24 hours.

3) DNN MODEL DEVELOPMENT

A Keras framework in Python programming language is employed to develop deep learning based on DNN architecture. To construct the DNN surrogate model required three steps: firstly, define the number of hidden layers, the number of neurons for each layer, an activation function, loss function, and a backpropagation optimizer algorithm. Secondly, the model must be trained with the training samples. In this study, the dataset is divided into three parts with an 80/10/10 ratio by using 80% for training, 10% for validation, and the remaining 10% for testing. Thirdly, try to reconfigure the network from the initial model that obtains the appropriate accuracy with the acceptable computation time. It should be noted that the performance of the model is evaluated using a mean absolute error (MAE) and a regression score (R-squared) as the accuracy measurement function. Finally, the DNN configuration that was used for the surrogate model in this study is shown in Table 1. More detail about how to organize deep learning using the Keras can be found in [60].

TABLE 1. The DNN configuration for the surrogate model.

Number of hidden layers	Number of neurons in each layer	Activate function	Loss function	Optimizer algorithm
5	300, 200, 200, 200, 50	ReLU	Mean square error (MSE)	Adam

B. THE PROPOSED SURROGATE ASSISTED MULTI-OBJECTIVE POPF

In this section, the outline of the proposed optimization framework, using surrogate assisted multi-objective POPF

(MO-POPF), is described. As mentioned in the above section, there are many objectives, constraints and non-linear functions. Therefore, the metaheuristic algorithm such as the multi-objective differential evolution is suitable for solving this problem.

1) MULTI-OBJECTIVE DIFFERENTIAL EVOLUTION

The multi-objective differential evolution (MODE) [61] is the algorithm that is widely used to find the appropriate solutions (near optimum) in complex optimization work [62]. Hence, the MODE algorithm is proposed to determine the optimal battery allocation in this study and its algorithm can be summarized as follows. Firstly, the algorithm is starting with the initial decision variables of the population which are randomly generated in the feasible space. Then, every individual sample is used to evaluate its fitness value. In this context, the individual input vector is obtained for the PPF calculation a total of 72 times (24 hours for each season). Next, all dominant candidates are discarded from the population using the non-dominated sorting technique. In this step, the remaining candidates are kept and randomly selected for generating the new offspring population using the differential evolution algorithm [63] which includes crossover, mutation, and selection. Once the process satisfies the termination criteria, the Pareto front will provide the candidate solutions. The flowchart of the MODE algorithm for solving the MO-POPF problem is presented in Fig. 3.

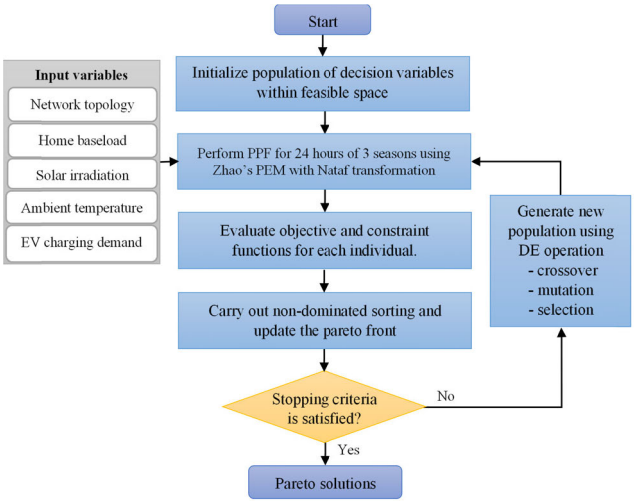

FIGURE 3. Multi-objective differential evolution algorithm for the POPF problem-solving.

2) OPTIMIZATION FRAMEWORK

The surrogate model can perform PPF computing faster when compared with using the AEM. However, the obtained solutions might lose the accuracy of the fitness functions compared to actual values. Hence, the optimal solutions from the surrogate model optimization should be verified and fine-tuned to be at acceptable accuracy. For this work, we have proposed the surrogate model to assist the optimization and the proposed framework is shown in Fig. 4.

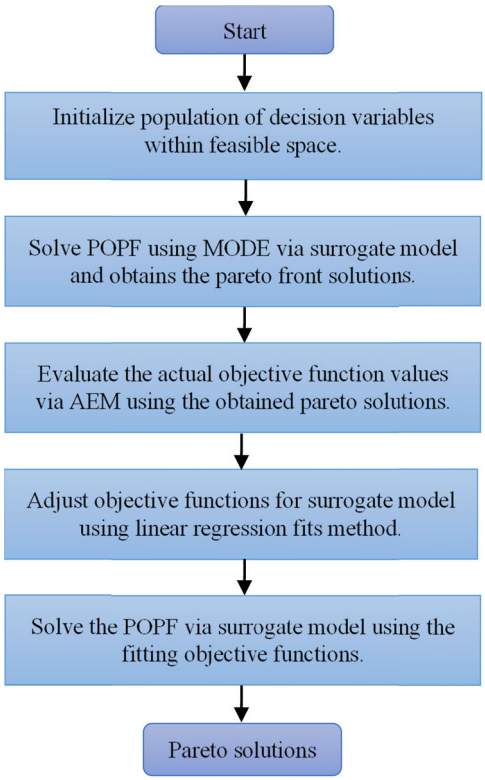

FIGURE 4. Surrogate-assisted multi-objective POPF framework.

As demonstrated in the optimization process shown in Fig. 4, the procedure starts with the random generation of the variable population in the feasible space. After that, the POPF solving process is performed using the MODE via the surrogate model. In the third step, the obtained Pareto solutions are carried out to calculate the real fitness function values using the AEM. Subsequently, both fitness function values obtained from the surrogate model and AEM are compared to determine the offset value. In this step, if the accuracy of the surrogate model is not satisfied, its calculated objective functions must be fine-tuned in the next step. In this paper, the linear regression fit model method is used to adjust the objective function as follows:

$$f'_{srg,i} = a_i + b_i f_{srg,i} \tag{47}$$

where $f'_{srg,i}$ is the adjusted value of the i^{th} objective function using surrogate model optimization while $f_{srg,i}$ is the calculated value of the actual i^{th} objective function in the previous optimizing step. Besides, a_i and b_i are the interception value and fitting slope coefficients, respectively.

Finally, the fitness evaluation of each Pareto solution is performed using the AEM to evaluate the actual objective values and then obtain the optimal BESS size and operation.

3) DECISION MAKING

The multi objectives optimization provides Pareto front with many optimal solutions. Therefore, it is required to select the best solution from all candidates that satisfy all

objectives. The best compromise solution can be provided using the fuzzy membership function approach [64], [65]. In this paper, the best trade-off solution between three considered objectives using the fuzzy function membership method is described as follows [64]:

$$SR = \sum_{i=1}^{N_f} \frac{f_i^{\max} - f_i(x_k)}{f_i^{\max} - f_i^{\min}}, \quad k \in \{1, 2, \ldots, N_s\} \qquad (48)$$

where f_i is the i^{th} objective function while x_k is the k^{th} candidate solution. $f_i^{\max}$ and $f_i^{\min}$ are the maximum and minimum values of the i^{th} objective function, respectively. N_f and N_s are the total number of the objective functions and the total number of the candidate solutions, respectively. SR is the comprehensive satisfaction rate of each solution set in the Pareto front solutions. Accordingly, the candidate solution (x_k) which makes the highest SR value is the best optimal compromise solution.

V. SIMULATION RESULTS

A. A CASE STUDY AND ASSUMPTIONS

In order to evaluate the performance of the proposed method, the typical radial distribution network in Udon Thani, Thailand, is used to perform in this study. This power system includes 36 buses and 27 households. The network connects to the main grid through a substation transformer of 100kVA, 22kV/400V. The single-line diagram of the understudy network is shown in Fig. 5. The structure of the low voltage network is the 3-phase, 4-wire overhead line system. The conductor configuration is UL3H95A (Aluminum conductor with PVC insulation material). The span of the main feeders is 40 meters while the span of each sub feeder is 20 meters. A specification of the substation transformer is shown in Table 2. Besides, the household load data of the understudy network are attached in Table 10 in Appendix A.

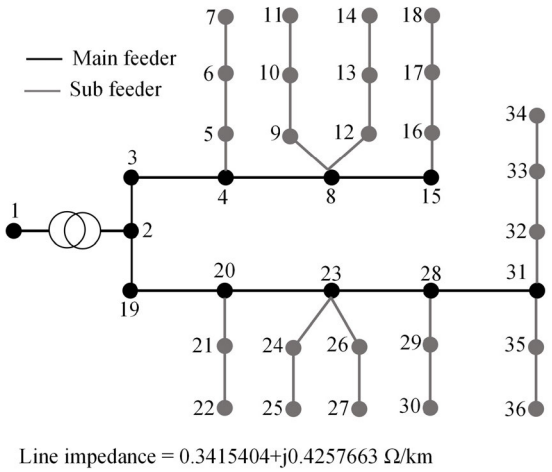

FIGURE 5. Single-line diagram of the understudy distribution system.

The local historical data over three years (2017-2020) of the hourly residential baseload is obtained from the automatic meter recording (AMR) system of the Provincial Electricity Authority (PEA) [66]. The ambient temperature data is obtained from the Thai Meteorological Department [67]. The hourly solar irradiation during the year 2015 to 2017 is provided by the Department of Alternative Energy Development and Efficiency, Ministry of Energy, Thailand [68]. Also, the solar PV module specification is obtained from the reference [69]. The monthly period of each season in this study denotes as follows: the winter season includes November - February. The summer season includes March - June and the remaining months (July - October) are in the rainy season. The load curve of each season is normalized by dividing the hourly baseload with the peak load value. Box plots of the hourly PDF for load demand, ambient temperature, and solar irradiation of each season are illustrated in Fig. 6, 7, and 8, respectively.

TABLE 2. The 100kVA transformer parameters.

Impedance = 5%	$\Delta\theta_r^{To} = 55$ °C	$\tau_o = 200$ min	$m = 0.8$
$R = 6.2$	$\Delta\theta_r^{H} = 25$ °C	$\tau_w = 7$ min	$n = 0.8$

TABLE 3. EVs vehicle specification.

EV Model	Proportion	Battery capacity (kWh)	Consumption (kWh/km)
Tesla Model 3	27%	62	0.17
Tesla Model S	25%	100	0.20
Chevy Volt	26%	18	0.22
Nissan Leaf	22%	40	0.16

To evaluate the hourly stochastic of EVs charging demand in the residential network following steps in Section 2, the historical traveling data from the National Household Travel Survey (NHTS) is obtained. The daily travel distance is randomly generated using a lognormal distribution function with a mean of 3.2 and the standard deviation with a value of 0.88. Also, regarding a report of the top EV sales by the model in the U.S. [70], four EV models namely Tesla Model 3 [71], Tesla Model S [72], Chevy Volt [73], and Nissan Leaf [74] are selected for this study and their specifications are listed in Table 3. The home charging power for all EVs is set at 3.3 kW with a unity power factor while the charging efficiency is 0.95. Also, the maximum number of iteration (Nmax) for the MCS running is 10,000. Accordingly, the probability of EVs charging in the box plot is demonstrated in Fig. 9.

Vanadium redox flow battery (VRFB) [75] is a kind of electrochemical energy storage that produces energy by using two tanks of liquid and two electrodes which are separated by an ion-exchange membrane. The main advantages of the VRFB are that it can offer almost unlimited energy capacity which could be useful for a long time charging and discharging. Hence, VRFB employment in the residential network

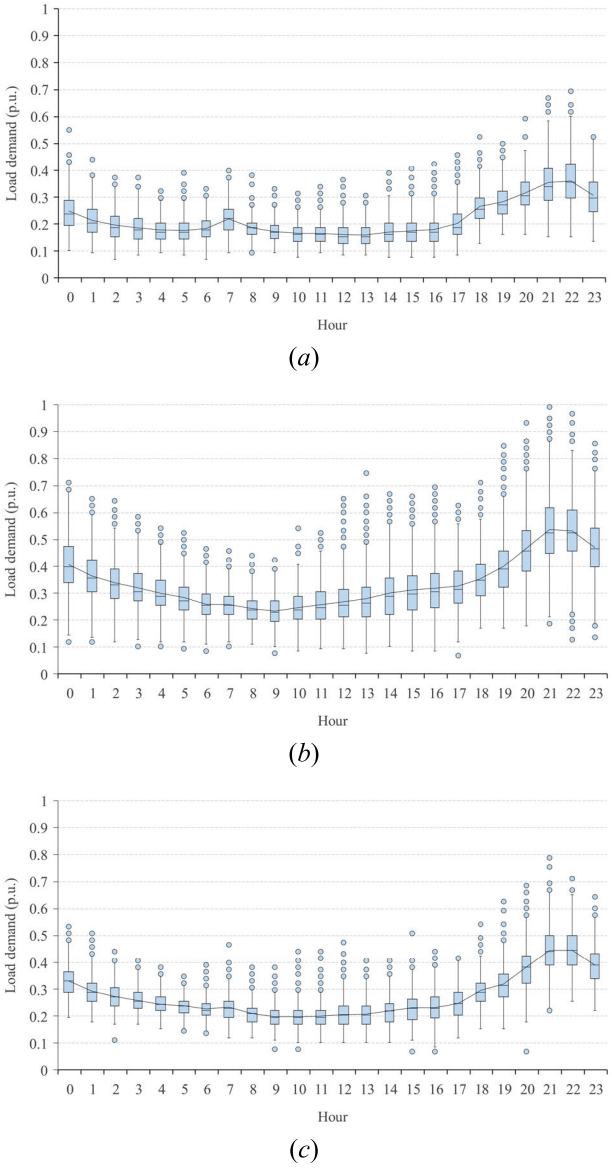

FIGURE 6. PDF of load demand; (a) Winter, (b) Summer and (c) Rainy.

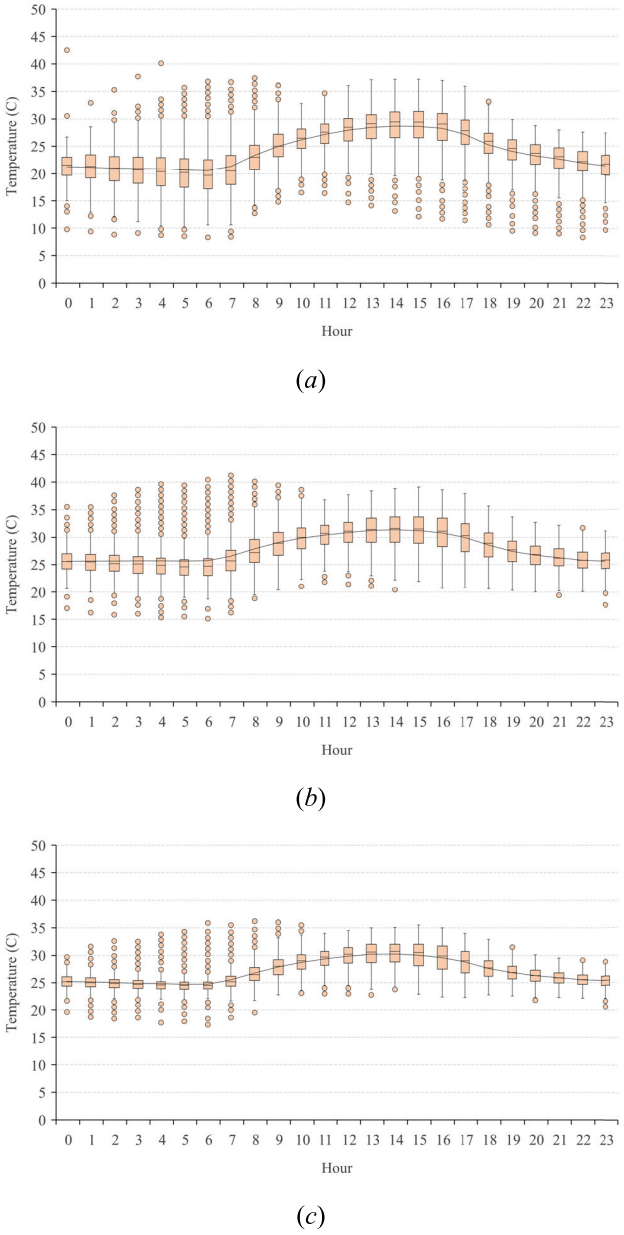

FIGURE 7. PDF of temperature; (a) Winter, (b) Summer and (c) Rainy.

with solar PV integration is cost-effective; consequently, it is selected as the BESS in this study. The VRFB specification and the economic parameters that relate to battery deployment cost is obtained from [10] and are shown in Table 4.

Lastly, the hourly carbon emission rate is varying based on fossil power plant generation. In this paper, the hourly carbon emission rate data is obtained from [76] and is shown in Fig. 10.

B. VERIFICATION OF THE METHODOLOGY

1) DNN SURROGATE MODEL VALIDATION

To verify the accuracy of the proposed DNN surrogate model. The surrogate model and the AEM are employed to evaluate the PPF calculation of the above-mentioned study case using the MCS method with 10,000 samples. The DNN surrogate model is developed in Python while the AEM is modeled in the PowerFactory. Both models run on a personal computer that has Intel core i7, 3.60GHz CPU, and 8GB of RAM. In this paper, each house is assumed to consist of a 5kW of solar PV rooftop and two EVs. The stochastics of hourly power demand for each house is supposed to be the same. The accuracy performance of the surrogate model and training time for the interesting output variables are attached in Table 5. Besides, the MCS is used to validate the PDF of load flow calculation between using the AEM and the surrogate model. The example simulation result of the substation transformer loading at the 23rd hour in summer is illustrated in Fig. 11.

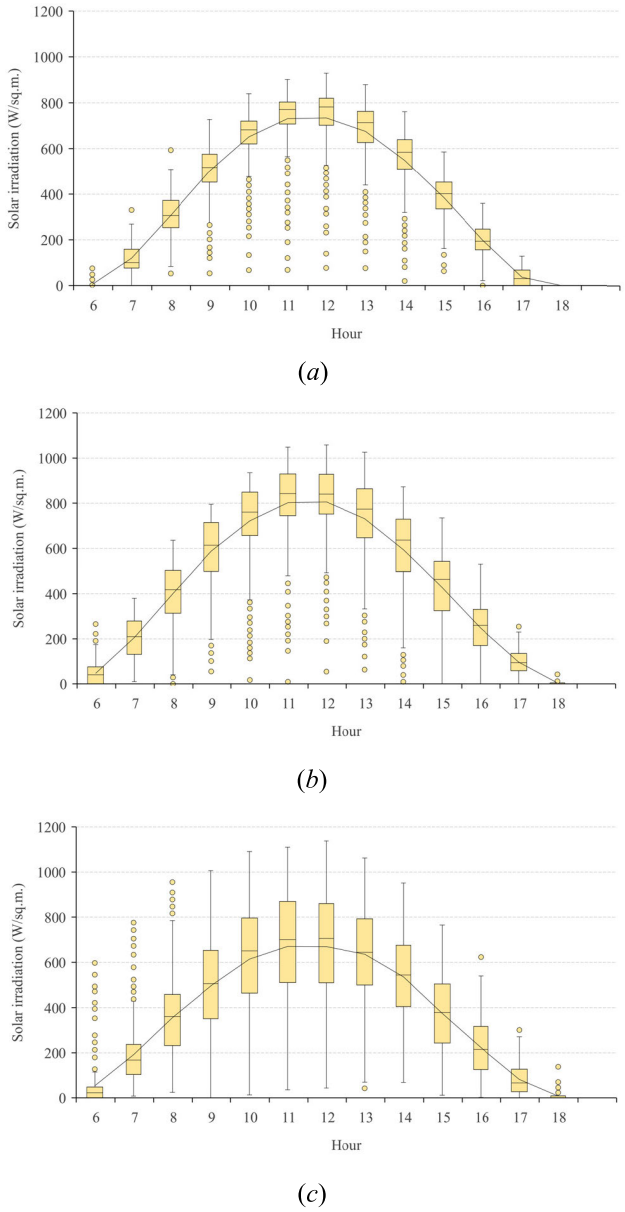

FIGURE 8. PDF of solar irradiation; (a) Winter, (b) Summer and (c) Rainy.

2) EVALUATION ON PPF CALCULATION METHOD

The MCS is well-known as the most accurate PPF analysis method when performing with enough large samples. This method is often used as the benchmark for other methods. Hence, in this section, the performance of the selected PEM method is compared with the MCS method to evaluate its effectiveness. The number of estimating points in Zhos' PEM is 5 points while the number of MCS samples is set to be 10,000. Both methods are used in this study using the actual model in the PowerFactory. The studied output variables include transformer loading, grid active power loss, current at the first branch (#2,3), and voltage at bus#18. Finally, the mean and standard deviation of the PDF output variables are evaluated and present in Table 6.

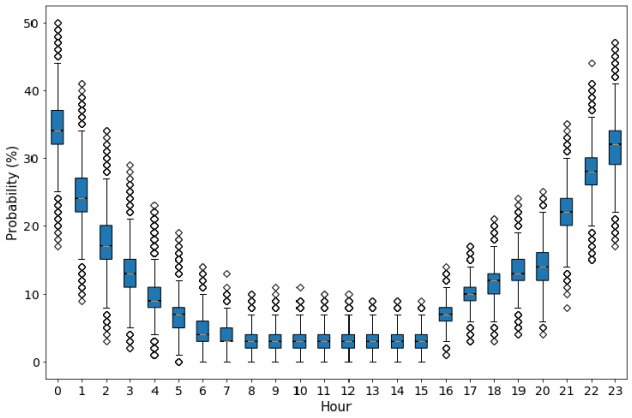

FIGURE 9. Probability of hourly EV charging at the resident.

TABLE 4. VRFB specification and economic parameters.

Parameter	Value	Parameter	Value
c_p	426$/kW	*%SoC min - max*	10 - 100%
c_e	100$/kWh	*Interest rate (r)*	3.00%
c_{Mp}	9$/kW	*Project lifetime (y)*	20 years
c_{Me}	0	*Cg-peak*	13.07 ¢/kWh
γ	0.8	*Cg-off peak*	8.14 ¢/kWh
$\eta_{b,c}$	0.85	*Cpv-peak*	5.25 ¢/kWh
$\eta_{d,c}$	0.80	*Cpv-off peak*	5.25 ¢/kWh

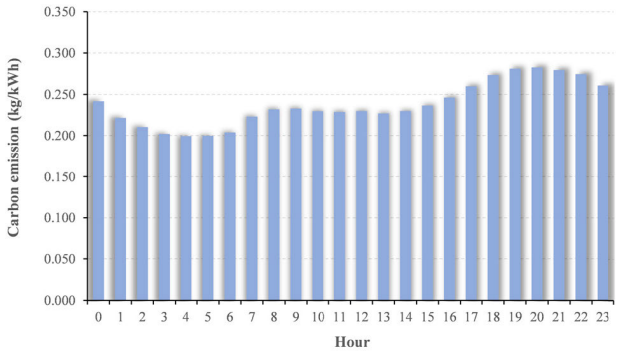

FIGURE 10. The hourly carbon emission rate.

According to the results in Fig. 11, the probability distribution of transformer loading in the active power (kW) using the AEM is presented in Fig. 11(a) while using the surrogate model is shown in Fig. 11(b). Besides, the probability distribution of transformer loading in apparent power (kVA) using the AEM is shown in Fig. 11(c), and using the surrogate model is presented in Fig. 11(d). It can be seen that the mean and standard deviation of the probability distribution of

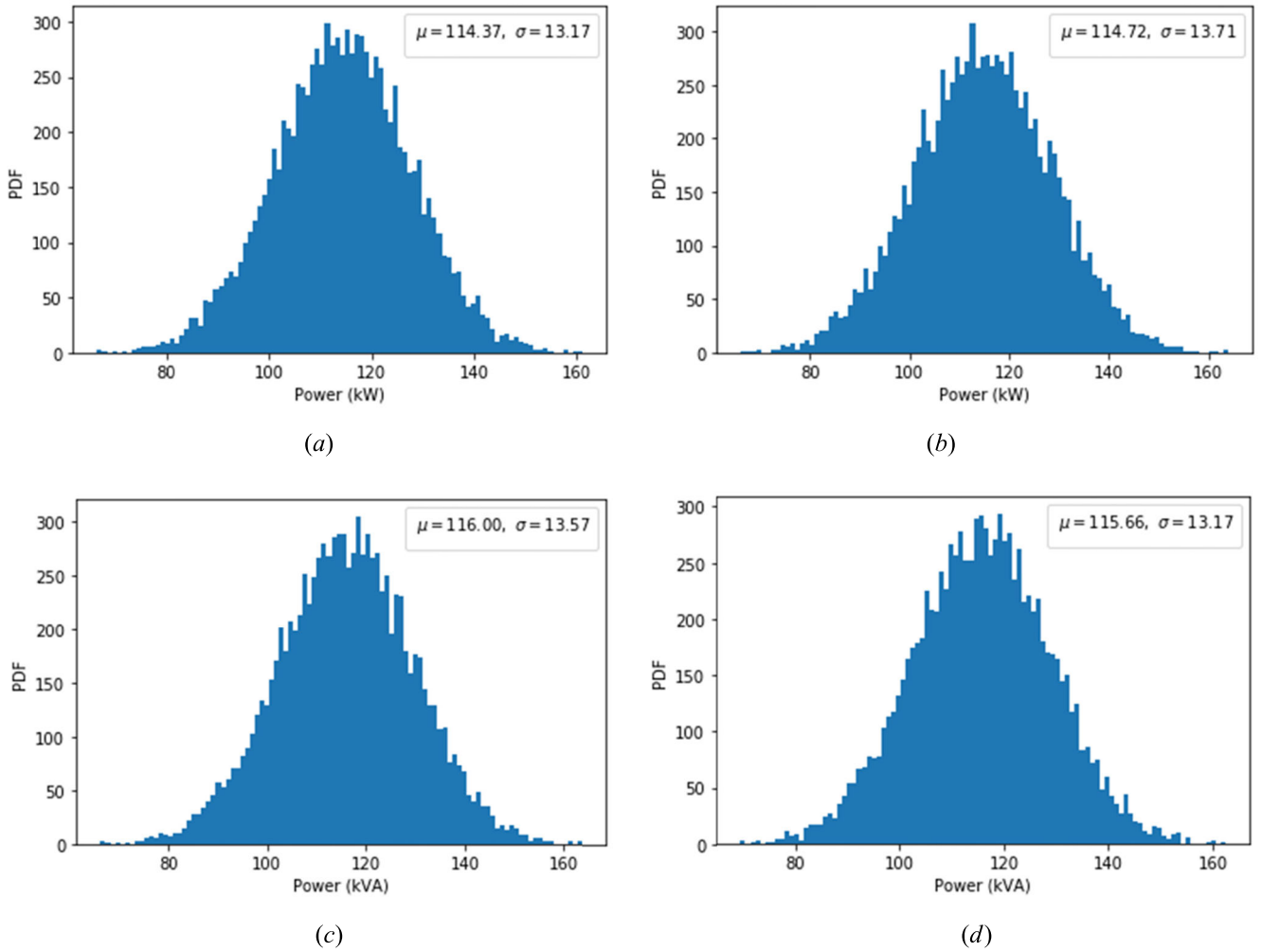

FIGURE 11. The PDF of transformer loading power at 23rd hour in summer, (a) Active power using AEM, (b) Active power using surrogate model, (c) Apparent power using AEM, and (d) Apparent power using the surrogate model.

TABLE 5. Accuracy and training time of the DNN surrogate models.

Surrogate model	Mean absolute error (MAE)	R-squared	Training time (sec.)
Transformer loading (kW)	0.87	0.9995	1,110
Transformer loading (kVA)	0.83	0.9990	1,113
Grid active power loss (kW)	0.12	0.9911	1,147
Current (branch#2,3)	4.41	0.8886	1,165
Voltage (bus#18)	0.98	0.9587	1,094

the active power and the apparent power using the surrogate model is very close to the AEM value.

It indicates that the surrogate model is appropriately constructed. From Table 6, the PPF of the interesting output variable including transformer loading, grid power loss, branch current, and bus voltage using the Zhos' PEM combined with Nataf transformation comparing with the MCS method is shown the acceptable error (less than 1% for the mean value and within ±3% for the standard deviation value). Therefore, it can be confirmed that using Zhao's PEM for the PPF calculation is an effective method.

C. SURROGATE ASSISTED MO-POPF PERFORMANCE

In this paper, the proposed surrogate-assisted multi-objective optimization framework is implemented in Python. The control parameters of MODE used in this paper are set as follows: the population size is 10 for three decision variables. The mutation method is the greedy strategy, namely best/1/bin while a scaling factor is 0.7. The crossover operation is a binomial crossover method with 0.8 of the crossover rates. Also, the maximum computation iteration is 200.

Regarding the methodology to find the optimal BESS location using the COG method as presented in Section 3. The BESS in the studied residential network is optimally installed at bus number 19. In this section, two scenarios

TABLE 6. PPF evaluation results using Zhao's PEM and MCS.

Output variable	Mean			Standard deviation		
	MCS	PEM	% Error	MCS	PEM	% Error
Transformer loading (kW)	114.37	115.44	0.94%	13.17	12.97	-1.52%
Transformer loading (kVA)	116.00	117.02	0.88%	13.57	13.38	-1.40%
Grid active power loss (kW)	2.13	2.14	0.47%	0.47	0.46	-2.13%
Current at branch#2,3 (A)	104.21	105.18	0.93%	16.13	16.54	2.54%
Voltage at bus#18 (V)	216.76	216.79	0.01%	1.94	1.99	2.58%

are used to evaluate the accuracy and performance of the proposed method. The first scenario is to validate the accuracy between the proposed surrogate-assisted method and the conventional method. The conventional method is defined as the surrogate-assisted optimization process without any fitting objective functions. The second scenario is to evaluate the performance of the MO-POPF using the proposed surrogate-assisted method and comparing with the optimization using the AEM.

In the first scenario, the POPF process was carried out using the surrogate model then the candidate solutions are carried out to calculate the fitness functions using the AEM. The mean absolute percentage error (MAPE) is used to measure the difference in fitness value between using the surrogate model and the AEM. As the numerical results presented in Fig. 12, the Pareto front using the surrogate model is shown in blue dot while the red dot represents the evaluated Pareto front using the AEM. The optimal Pareto solutions using the conventional surrogate-assisted is illustrated in Fig. 12(a) while Fig. 12(b) presents the Pareto solutions using the proposed surrogate-assisted MO-POPF method. In addition, the comparison of the accuracy of the Pareto solution based on the MAPEs indicator between the proposed surrogate-assisted method and the conventional method is presented in Table 7.

TABLE 7. Pareto solutions accuracy obtaining from the conventional method and the proposed method.

Objective function	Mean absolute percentage error (MAPE)	
	Conventional method	Proposed method
f_1	0.1574%	0.0006%
f_2	4.2123%	0.0138%
f_3	0.1398%	0.0003%

In the second scenario, the MO-POPF is performed to determine the optimal BESS allocation using two methods. For the first method, the optimization was done using the AEM while in the second method it was done using the proposed surrogate-assisted MO-POPF. The maximum iteration of the optimization process is set to be 200. Then the minimum value of each objective function and the computation time from using the above methods are obtained. The comparison of the minimum fitness value and the computation time between using the proposed surrogate-assisted and the AEM is shown in Table 8.

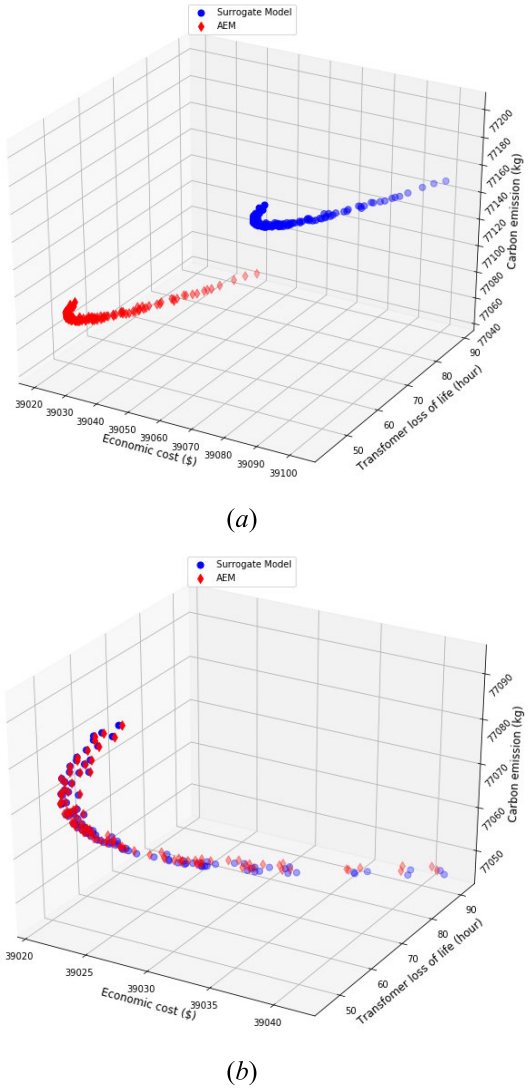

FIGURE 12. Pareto optimal front of the multi-objective BESS sizing and operation problem, (a) Conventional method (without objective function fitting), and (b) The proposed method using objective function fitting.

TABLE 8. Comparison of the fitness value and the computation time between using AEM and the surrogate-assisted optimization.

Objective function	f_1	f_2	f_3	Computation time (hour)
AEM	39,004.62	46.12	76,920.31	508.48
Surrogate-assist	39,020.99	45.65	77,045.66	57.20
% different	0.04%	-1.01%	0.16%	88.76%

In Fig. 12, the Pareto front using the proposed surrogate-assisted framework is very close to the Pareto front using the AEM. Also, when evaluating the accuracy of the Pareto solutions using the proposed surrogate-assisted method compares with the former surrogate-assisted as shown in Table 7, the MAPE using the former method varies about $0.1398 - 4.2123\%$ whereas the range of the MAPE value using the proposed method is only $0.0003 - 0.0138\%$. Thus, the proposed surrogate-assisted optimization method presents higher accuracy. In Table 8, the computation time to determine the minimum solution for each objective function for the MO-POPF problem based on using the AEM is over 508 hours while the computation time when using the proposed method is only 57 hours. The computation time of the optimization can be reduced by about 88%. Besides, the fitness value differs from using the AEM by only $\pm 1\%$.

D. OPTIMAL BESS ALLOCATION

To find the optimal BESS allocation in the distribution network considering many objectives in this study. The best trade-off solution obtained from using the proposed surrogate-assisted MO-POPF method is carried out to perform in the actual model to determine the real optimal BESS discharging power threshold (kW). Then the BESS sizing in kW and kWh capacity are calculated. The minimizing of three objective functions including the economic cost, transformer loss of life, and the carbon emission are evaluated. The base case scenario in terms of without any BESS implementation in the study network case is set to use for comparison with the proposed optimization method.

In Table 9, the optimal BESS allocation in the distribution system is presented. The optimized BESS discharging power thresholds in winter, summer, and rainy seasons are 54.50 kW, 73.15 kW, and 70.34 kW, respectively. The optimal sizing of the BESS power rating is 39.82 kW while its energy capacity rating is 188.86 kWh. The probabilistic evaluations of the three objective functions are done for the base case and the optimized BESS installation case. In the first objective, the economic cost is 40,896.41$ per year for the base case, while using the optimal BESS allocation case the annual cost goes down to 39,021.12$. In the second objective function, the transformer loss of life rises to 257.99 hours per year for the base case. However, the optimal case shows a significant reduction in the transformer aging and it is 53.77 hours per year. Lastly, the annual carbon emission is considered in the third objective. In the base case, the residential energy consumption emits carbon into the environment about 90,383.77 kg per year. However, using the proposed optimal BESS to manage the surplus PV generation power can down the carbon emission to be 77,062.50 kg.

E. IMPACT ON THE TRANSFORMER LOSS OF LIFE

The expected values of the transformer winding hottest-spot temperature for the base case and the optimal BESS allocation case are presented in Fig. 13. Also, the probability of the winding hottest-spot temperature evaluation based on Zhao's PEM calculation for both cases is illustrated in Fig. 14. The result shows that the maximum temperature for the base case of the transformer winding hottest-spot temperature is at the 23^{rd} hour in the summer. Whereas, the optimal case shows its maximum value at the midnight hour in the summer. It is also observed that the winding hottest-spot temperature of the base case can go over 110°C that means the transformer operation capacity can deteriorate. However, in the optimal case, the winding hottest-spot temperature can be controlled within the safe operating range.

VI. DISCUSSION

The probabilistic optimization for the power system planning requires substantial computational time, especially when considering many uncertain variables. Therefore, this study proposes the new surrogate-assisted optimization method to improve accuracy and reduce the computation burden. The accuracy is improved by the surrogate-assisted method through the tuning of fitness function while at the same time determination of the minimum solution reduces the computation time. In this paper, the DNN surrogate model is introduced to replace the mathematical load flow calculation in the power system which takes more time for iterative computation. According to the evaluation results in Table 5 and Fig. 11, it can be proved that the DNN surrogate model can be used for obtaining the load flow calculation with the acceptable accuracy balancing with the training time.

The proposed surrogate-assisted optimization method has been evaluated on both accuracy and performance. For evaluation, the proposed method is applied in the distribution network and then compared with results using the conventional surrogate-assisted optimization method. From the results, shown in Fig. 11 and Table 7, it can be seen that the Pareto solutions using the proposed surrogate-assisted method are very close to the Pareto solutions using the actual model. In addition, the accuracy obtained by the proposed method is higher than the former surrogate-assisted optimization method. This is because the proposed surrogate-assisted method is added into the process to tune the obtained fitness function value from the surrogate model to fit with the actual value while the former surrogate-assisted method does not have this option. Moreover, the optimization results listed in Table 8, clearly show that the proposed method can

TABLE 9. Optimal BESS solution and objective values.

Case	BESS discharging power threshold (kW)			BESS power rating (kW)	BESS energy capacity (kWh)	Economic cost ($)	Transformer loss of life (hours)	Carbon emission (kg)
	Winter	Summer	Rainy					
Base case	-	-	-	-	-	40,896.41	257.99	90,383.77
Optimal BESS allocation case	54.50	73.15	70.34	39.82	188.86	39,021.12	53.77	77,062.50
Reduction	-	-	-	-	-	4.59%	79.16%	14.74%

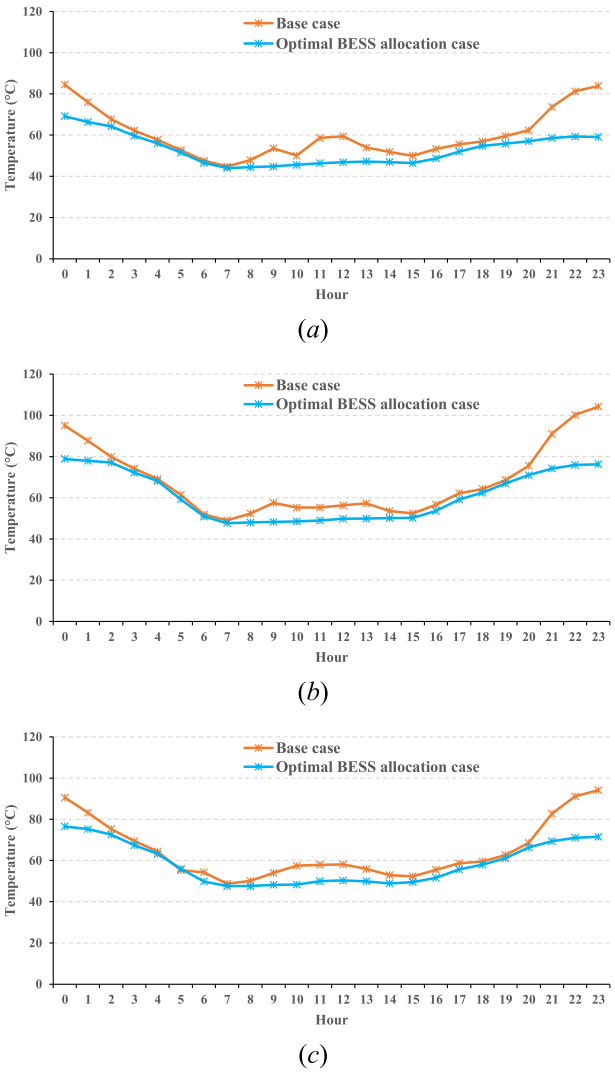

FIGURE 13. The expected value of the transformer winding hottest-spot temperature; (a) Winter, (b) Summer and (c) Rainy.

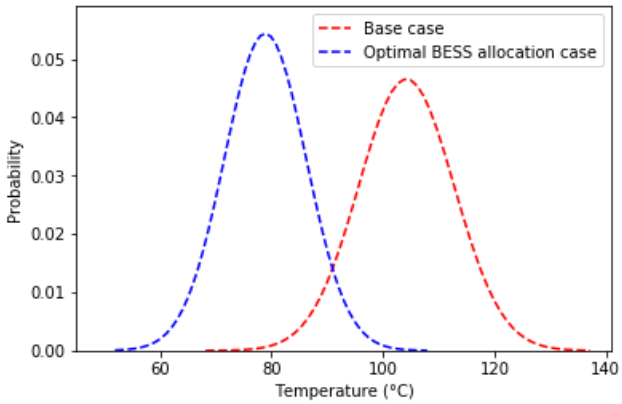

FIGURE 14. Probabilities of the transformer winding hottest-spot temperature at the 23rd hour in summer; (a) Base case and (b) Optimal BESS allocation case.

determine the minimum solution which is close to the results from the optimization process using the actual model while at the same time, the proposed method consumes about 88% less computation time than the computation time necessary using the actual model. These results confirm that the proposed surrogate-assisted method is very effective in mitigating the heavy computation burden in the MO-POPF work.

Results in Table 9 demonstrate the effectiveness of the proposed surrogate-assisted MO-POPF method. The BESS allocation in the distribution network with solar PVs and EVs using the proposed optimization method can reduce the annual economic cost, significantly save the transformer loss of life and reduce the carbon emission to the atmosphere. The better performance and the simple method of the new surrogate-assisted framework can also be applied to the other optimization works especially in the probabilistic optimal planning problem.

VII. CONCLUSION

The new surrogate-assisted probabilistic multi-objective OPF method for the distribution network considering various uncertain sources including solar irradiation, ambient temperature, residential baseload, and EVs charging power demand has been proposed in this paper. Also, the probability of EVs charging in the residential network affected by the TOU electricity rate is evaluated based on the MCS method. Zhao's

TABLE 10. Households load data.

House no.	Location (bus no.)	Phase	Max. load (kW)
1	3	*a*	6
2	5	*a*	6
3	6	*b*	5
4	7	*c*	6
5	9	*a*	6
6	10	*b*	6
7	11	*c*	5
8	12	*a*	6
9	13	*b*	5
10	14	*c*	4
11	16	*a*	6
12	17	*b*	5
13	18	*c*	4
14	19	*b*	4
15	21	*c*	5
16	22	*a*	5
17	24	*b*	4
18	25	*c*	6
19	26	*a*	5
20	27	*b*	6
21	29	*c*	4
22	30	*a*	6
23	32	*a*	6
24	33	*b*	5
25	34	*c*	4
26	35	*b*	4
27	36	*c*	6

PEM is used to perform the probabilistic power flow calculation while using the Nataf transformation to deal with the correlation of the input random variables. The BESS is adopted to do the POPF in the distribution system with solar PVs and EVs. The optimal location for the BESS installation is determined using the COG method. The battery operating strategy includes battery charging operation with the surplus power from solar PVs generation and the discharge operation controlled by the optimized discharging power threshold. Three optimization objectives are formulated including economic cost, transformer loss of life, and carbon emission. Also, the security chance constraints of the network safe operation is considered.

To overcome the expensive computational time required for the optimal BESS allocation based on the probabilistic load flow calculation, the surrogate-assisted optimization method is applied. The surrogate model is developed by using deep learning namely DNN which is used to estimate the deterministic power flow calculation. To demonstrate the effectiveness of the proposed method, the typical radial distribution network in Udon Thani, Thailand, is performed. Besides, the local historical data including solar irradiation, ambient temperature, and residential baseload is used while the EV travel data is obtained from the NHTS. The numerical result shows that the proposed surrogate-assisted optimization method can provide the Pareto front for the BESS allocation which gives the objective values very close to the values obtained by using the actual model. The new surrogate-assisted optimization method has been shown more accurate than the conventional method. Moreover, the required computation time for the probabilistic multi-objective OPF can be reduced by over 88% when comparing with using the actual model in the optimization process. Finally, the best trade-off solution between the three objective functions using the fuzzy membership function method shows the reductions of the annual economic cost, transformer loss of life, and carbon emission by 4.59%, 79.16% and 14.74% from the base case, respectively. Besides, the network operation such as the transformer winding hottest-spot temperature can be controlled within the safe operation limit at a high probability. Simulation results confirm the effectiveness of the proposed methodology. The significant performance improvement in the calculation using the proposed surrogate-assisted optimization method opens up avenues for its potential use in future studies on energy system optimization such as the real-time optimization in the power system under uncertain environment.

APPENDIX

A. APPENDIX A

See table 10.

ACKNOWLEDGMENT

The authors would like to thank Assoc.Prof. Dr. Surachai Chaitusaney from the Department of Electrical Engineering, Chulalongkorn University, Thailand, for useful advice on the instruction and discussion of this article.

REFERENCES

[1] IRENA. (2020). *Renewable Power Generation Costs in 2019, International Renewable Energy Agency, Abu Dhabi*. Accessed: Jun. 2020. [Online]. Available: https://www.irena.org/publications/2020/Jun/Renewable-Power-Costs-in-2019

[2] IEA. (2020). *Global EV Outlook 2020, IEA, Paris*. [Online]. Available: https://www.iea.org/reports/global-ev-outlook-2020.

[3] United Nations. (2015). *The Paris Agreement, UNFCCC*. [Online]. Available:https://sustainabledevelopment.un.org/content/documents/17853parisagreement.pdf

[4] Y. Yang, S. Bremner, C. Menictas, and M. Kay, "Battery energy storage system size determination in renewable energy systems: A review," *Renew. Sustain. Energy Rev.*, vol. 91, pp. 109–125, Aug. 2018, doi: 10.1016/j.rser.2018.03.047.

[5] G. J. May, A. Davidson, and B. Monahov, "Lead batteries for utility energy storage: A review," *J. Energy Storage*, vol. 15, pp. 145–157, Feb. 2018, doi: 10.1016/j.est.2017.11.008.

[6] H. Hesse, R. Martins, P. Musilek, M. Naumann, C. Truong, and A. Jossen, "Economic optimization of component sizing for residential battery storage systems," *Energies*, vol. 10, no. 7, p. 835, Jun. 2017, doi: 10.3390/en10070835.
[7] G. R. Barai, B. Venkatesh, and M. A. Awadallah, "Optimization of hybrid energy storage systems for power curve smoothening at grid scale," *Can. J. Electr. Comput. Eng.*, vol. 41, no. 2, pp. 87–94, 2018, doi: 10.1109/CJECE.2018.2836860.
[8] M. El-Hendawi, H. A. Gabbar, G. El-Saady, and E. N. A. Ibrahim, "Control and EMS of a grid-connected microgrid with economical analysis," *Energies*, vol. 11, no. 1, pp. 1–20, 2018, doi: 10.3390/en11010129.
[9] N. Khaboot, C. Srithapon, A. Siritaratiwat, and P. Khunkitti, "Increasing benefits in high PV penetration distribution system by using battery enegy storage and capacitor placement based on salp swarm algorithm," *Energies*, vol. 12, no. 24, p. 4817, Dec. 2019, doi: 10.3390/en12244817.
[10] M. R. Jannesar, A. Sedighi, M. Savaghebi, and J. M. Guerrero, "Optimal placement, sizing, and daily charge/discharge of battery energy storage in low voltage distribution network with high photovoltaic penetration," *Appl. Energy*, vol. 226, pp. 957–966, Sep. 2018, doi: 10.1016/j.apenergy.2018.06.036.
[11] S. Surender Reddy and P. R. Bijwe, "Day-ahead and real time optimal power flow considering renewable energy resources," *Int. J. Electr. Power Energy Syst.*, vol. 82, pp. 400–408, Nov. 2016, doi: 10.1016/j.ijepes.2016.03.033.
[12] H. Khorramdel, J. Aghaei, B. Khorramdel, and P. Siano, "Optimal battery sizing in microgrids using probabilistic unit commitment," *IEEE Trans. Ind. Informat.*, vol. 12, no. 2, pp. 834–843, Apr. 2016, doi: 10.1109/TII.2015.2509424.
[13] S. A. Alavi, A. Ahmadian, and M. Aliakbar-Golkar, "Optimal probabilistic energy management in a typical micro-grid based-on robust optimization and point estimate method," *Energy Convers. Manage.*, vol. 95, pp. 314–325, May 2015.
[14] R. A. Thokar, N. Gupta, K. R. Niazi, A. Swarnkar, S. Sharma, and K. Meena, "Optimal integration and management of solar generation and battery storage system in distribution systems under uncertain environment," *Int. J. Renew. Energy Res.*, vol. 10, no. 1, pp. 11–12, 2020.
[15] H. Wang, Z. Yan, M. Shahidehpour, Q. Zhou, and X. Xu, "Optimal energy storage allocation for mitigating the unbalance in active distribution network via uncertainty quantification," *IEEE Trans. Sustain. Energy*, vol. 12, no. 1, pp. 303–313, Jan. 2021, doi: 10.1109/TSTE.2020.2992960.
[16] U. H. Ramadhani, M. Shepero, J. Munkhammar, J. Widén, and N. Etherden, "Review of probabilistic load flow approaches for power distribution systems with photovoltaic generation and electric vehicle charging," *Int. J. Electr. Power Energy Syst.*, vol. 120, Sep. 2020, Art. no. 106003, doi: 10.1016/j.ijepes.2020.106003.
[17] Z. Ullah, S. Wang, J. Radosavljevic, and J. Lai, "A solution to the optimal power flow problem considering WT and PV generation," *IEEE Access*, vol. 7, pp. 46763–46772, 2019, doi: 10.1109/ACCESS.2019.2909561.
[18] M. J. Morshed, J. B. Hmida, and A. Fekih, "A probabilistic multi-objective approach for power flow optimization in hybrid wind-PV-PEV systems," *Appl. Energy*, vol. 211, pp. 1136–1149, Feb. 2018, doi: 10.1016/j.apenergy.2017.11.101.
[19] C. Chen, W. Wu, B. Zhang, and H. Sun, "Correlated probabilistic load flow using a point estimate method with nataf transformation," *Int. J. Electr. Power Energy Syst.*, vol. 65, pp. 325–333, Feb. 2015, doi: 10.1016/j.ijepes.2014.10.035.
[20] Y. M. Atwa, E. F. El-Saadany, M. M. A. Salama, and R. Seethapathy, "Optimal renewable resources mix for distribution system energy loss minimization," *IEEE Trans. Power Syst.*, vol. 25, no. 1, pp. 360–370, Feb. 2010, doi: 10.1109/TPWRS.2009.2030276.
[21] J. Sardi, N. Mithulananthan, and D. Q. Hung, "Strategic allocation of community energy storage in a residential system with rooftop PV units," *Appl. Energy*, vol. 206, pp. 159–171, Nov. 2017, doi: 10.1016/j.apenergy.2017.08.186.
[22] G. Li and X.-P. Zhang, "Modeling of plug-in hybrid electric vehicle charging demand in probabilistic power flow calculations," *IEEE Trans. Smart Grid*, vol. 3, no. 1, pp. 492–499, Mar. 2012, doi: 10.1109/TSG.2011.2172643.
[23] Z. Liu, J. Yang, Y. Zhang, T. Ji, J. Zhou, and Z. Cai, "Multi-objective coordinated planning of active-reactive power resources for decentralized droop-controlled islanded microgrids based on probabilistic load flow," *IEEE Access*, vol. 6, pp. 40267–40280, 2018, doi: 10.1109/ACCESS.2018.2855697.
[24] Q. Xiao, "Comparing three methods for solving probabilistic optimal power flow," *Electr. Power Syst. Res.*, vol. 124, pp. 92–99, Jul. 2015, doi: 10.1016/j.epsr.2015.03.001.
[25] S. Shargh, B. K. Ghazani, B. Mohammadi-ivatloo, H. Seyedi, and M. Abapour, "Probabilistic multi-objective optimal power flow considering correlated wind power and load uncertainties," *Renew. Energy*, vol. 94, pp. 10–21, Aug. 2016, doi: 10.1016/j.renene.2016.02.064.S.
[26] S. Zeynali, N. Rostami, and M. R. Feyzi, "Multi-objective optimal short-term planning of renewable distributed generations and capacitor banks in power system considering different uncertainties including plug-in electric vehicles," *Int. J. Electr. Power Energy Syst.*, vol. 119, Jul. 2020, Art. no. 105885, doi: 10.1016/j.ijepes.2020.105885.
[27] W. P. J. Philippe, S. Zhang, S. Eftekharnejad, P. K. Ghosh, and P. K. Varshney, "Mixed copula-based uncertainty modeling of hourly wind farm production for power system operational planning studies," *IEEE Access*, vol. 8, pp. 138569–138583, 2020, doi: 10.1109/ACCESS.2020.3012437.
[28] F. Ni, P. H. Nguyen, and J. F. G. Cobben, "Basis-adaptive sparse polynomial chaos expansion for probabilistic power flow," *IEEE Trans. Power Syst.*, vol. 32, no. 1, pp. 694–704, Jan. 2017, doi: 10.1109/TPWRS.2016.2558622.
[29] X. Xu, Z. Yan, M. Shahidehpour, S. Chen, H. Wang, Z. Li, and Q. Zhou, "Maximum loadability of islanded microgrids with renewable energy generation," *IEEE Trans. Smart Grid*, vol. 10, no. 5, pp. 4696–4705, Sep. 2019, doi: 10.1109/TSG.2018.2848958.
[30] K. Wansaseub, S. Sleesongsom, N. Panagant, N. Pholdee, and S. Bureerat, "Surrogate-assisted reliability optimisation of an aircraft wing with static and dynamic aeroelastic constraints," *Int. J. Aeronaut. Space Sci.*, vol. 21, no. 3, pp. 723–732, Sep. 2020, doi: 10.1007/s42405-019-00246-6.
[31] D. Coppitters, W. De Paepe, and F. Contino, "Surrogate-assisted robust design optimization and global sensitivity analysis of a directly coupled photovoltaic-electrolyzer system under techno-economic uncertainty," *Appl. Energy*, vol. 248, pp. 310–320, Aug. 2019, doi: 10.1016/j.apenergy.2019.04.101.
[32] H. R. Baghaee, M. Mirsalim, G. B. Gharehpetian, and H. A. Talebi, "Application of RBF neural networks and unscented transformation in probabilistic power-flow of microgrids including correlated wind/PV units and plug-in hybrid electric vehicles," *Simul. Model. Pract. Theory*, vol. 72, pp. 51–68, Mar. 2017, doi: 10.1016/j.simpat.2016.12.006.
[33] T. Kunakote and S. Bureerat, "Surrogate-assisted multiobjective evolutionary algorithms for structural shape and sizing optimisation," *Math. Probl. Eng.*, vol. 2013, pp. 21–23, Jan. 2013, doi: 10.1155/2013/695172.
[34] C. Vidal, P. Malysz, P. Kollmeyer, and A. Emadi, "Machine learning applied to electrified vehicle battery state of charge and state of health estimation: State-of-the-art," *IEEE Access*, vol. 8, pp. 52796–52814, 2020, doi: 10.1109/ACCESS.2020.2980961.
[35] A. T. D. Perera, P. U. Wickramasinghe, V. M. Nik, and J.-L. Scartezzini, "Machine learning methods to assist energy system optimization," *Appl. Energy*, vol. 243, pp. 191–205, Jun. 2019, doi: 10.1016/j.apenergy.2019.03.202.
[36] C. Wang, C. Liu, F. Tang, D. Liu, and Y. Zhou, "A scenario-based analytical method for probabilistic load flow analysis," *Electr. Power Syst. Res.*, vol. 181, Apr. 2020, Art. no. 106193, doi: 10.1016/j.epsr.2019.106193.
[37] N. Gupta, "Gauss-Quadrature-Based probabilistic load flow method with voltage-dependent loads including WTGS, PV, and EV charging uncertainties," *IEEE Trans. Ind. Appl.*, vol. 54, no. 6, pp. 6485–6497, Nov. 2018, doi: 10.1109/TIA.2018.2855164.
[38] S. S. Reddy, A. R. Abhyankar, and P. R. Bijwe, "Market clearing for a wind-thermal power system incorporating wind generation and load forecast uncertainties," in *Proc. IEEE Power Energy Soc. Gen. Meeting*, Jul. 2012, pp. 1–8, doi: 10.1109/PESGM.2012.6345335.
[39] J. Park, W. Liang, J. Choi, A. A. El-Keib, M. Shahidehpour, and R. Billinton, "A probabilistic reliability evaluation of a power system including solar/photovoltaic cell generator," in *Proc. IEEE Power Energy Soc. Gen. Meeting PES*, Jul. 2009, pp. 1–6, doi: 10.1109/PES.2009.5275722.
[40] E. Grover-Silva, M. Heleno, S. Mashayekh, G. Cardoso, R. Girard, and G. Kariniotakis, "A stochastic optimal power flow for scheduling flexible resources in microgrids operation," *Appl. Energy*, vol. 229, pp. 201–208, Nov. 2018, doi: 10.1016/j.apenergy.2018.07.114.
[41] M. Fan, V. Vittal, G. T. Heydt, and R. Ayyanar, "Probabilistic power flow studies for transmission systems with photovoltaic generation using cumulants," *IEEE Trans. Power Syst.*, vol. 27, no. 4, pp. 2251–2261, Nov. 2012, doi: 10.1109/TPWRS.2012.2190533.

[42] (2009). *National Household Travel Survey (NHTS). USA Department Transportation*. Washington, DC, USA. [Online]. Available: www.nhts.ornl.gov

[43] T. Wu, Q. Yang, Z. Bao, and W. Yan, "Coordinated energy dispatching in microgrid with wind power generation and plug-in electric vehicles," *IEEE Trans. Smart Grid*, vol. 4, no. 3, pp. 1453–1463, Sep. 2013, doi: 10.1109/TSG.2013.2268870.

[44] K. Qian, C. Zhou, M. Allan, and Y. Yuan, "Modeling of load demand due to EV battery charging in distribution systems," *IEEE Trans. Power Syst.*, vol. 26, no. 2, pp. 802–810, May 2011, doi: 10.1109/TPWRS.2010.2057456.

[45] C. Wu, F. Wen, Y. Lou, and F. Xin, "Probabilistic load flow analysis of photovoltaic generation system with plug-in electric vehicles," *Int. J. Electr. Power Energy Syst.*, vol. 64, pp. 1221–1228, Jan. 2015, doi: 10.1016/j.ijepes.2014.09.014.

[46] Y. G. Zhao and T. Ono, "New point estimates for probability moments," *J. Eng. Mech.*, vol. 126, no. 4, pp. 1998–2001, 2000, doi: 10.1061/(ASCE)0733-9399(2000)126:4(433).

[47] M. Mohammadi, A. Shayegani, and H. Adaminejad, "A new approach of point estimate method for probabilistic load flow," *Int. J. Electr. Power Energy Syst.*, vol. 51, pp. 54–60, Oct. 2013, doi: 10.1016/j.ijepes.2013.02.019.

[48] H. Li, Z. Lü, and X. Yuan, "Nataf transformation based point estimate method," *Sci. Bull.*, vol. 53, no. 17, pp. 2586–2592, Sep. 2008, doi: 10.1007/s11434-008-0351-0.

[49] P. Ling and A. D. Kiureghian, "Multivariate distribution models with prescribed marginals and covariances," *Probabilistic Eng. Mech.*, vol. 1, no. 2, pp. 105–112, Jun. 1986, doi: 10.1016/0266-8920(86)90033-0.

[50] C. Wang and C.-Y. Hsu, "Rankings correlation study: Brand search volume vs. Brand sales volume," in *Proc. 5th IEEE Int. Conf. Big Data Anal. (ICBDA)*, May 2020, pp. 6–10, doi: 10.1109/ICBDA49040.2020.9101286.

[51] *IEEE Guide for Loading Mineral-Oil-Immersed Transformers and Step-Voltage Regulators*, Standard IEEE Std C57.91-2011 (Revision of IEEE Std C57.91-1995), Mar. 2012, pp. 1–123, doi: 10.1109/IEEESTD.2012.6166928.

[52] M. R. Sarker, D. J. Olsen, and M. A. Ortega-Vazquez, "Co-optimization of distribution transformer aging and energy arbitrage using electric vehicles," *IEEE Trans. Smart Grid*, vol. 8, no. 6, pp. 2712–2722, Nov. 2017, doi: 10.1109/TSG.2016.2535354.

[53] M. Kaplan and A. Braunstein, "Contribution to the determination of the optimum site for substations," *IEEE Power Eng. Rev.*, vol. PER-1, no. 5, pp. 27–28, May 1981, doi: 10.1109/MPER.1981.5511508.

[54] H. Gu, Y.-P. Xu, D. Ma, J. Xie, L. Liu, and Z. Bai, "A surrogate model for the variable infiltration capacity model using deep learning artificial neural network," *J. Hydrol.*, vol. 588, Sep. 2020, Art. no. 125019, doi: 10.1016/j.jhydrol.2020.125019.

[55] W. Zhu, J. Chebeir, and J. A. Romagnoli, "Operation optimization of a cryogenic NGL recovery unit using deep learning based surrogate modeling," *Comput. Chem. Eng.*, vol. 137, Jun. 2020, Art. no. 106815, doi: 10.1016/j.compchemeng.2020.106815.

[56] J. Tao and G. Sun, "Application of deep learning based multi-fidelity surrogate model to robust aerodynamic design optimization," *Aerosp. Sci. Technol.*, vol. 92, pp. 722–737, Sep. 2019, doi: 10.1016/j.ast.2019.07.002.

[57] PowerFactory. (2019). *PowerFactory 2019*. Germany. [Online]. Available: https://www.digsilent.de/en/downloads.html

[58] L. Alvarado-Barrios, C. Alvarez-Arroyo, J. M. Escano, F. M. Gonzalez-Longatt, and J. L. Martinez-Ramos, "Two-level optimisation and control strategy for unbalanced active distribution systems management," *IEEE Access*, vol. 8, pp. 197992–198009, 2020, doi: 10.1109/ACCESS.2020.3034446.

[59] Z. Shu and P. Jirutitijaroen, "Latin hypercube sampling techniques for power systems reliability analysis with renewable energy sources," *IEEE Trans. Power Syst.*, vol. 26, no. 4, pp. 2066–2073, Nov. 2011, doi: 10.1109/TPWRS.2011.2113380.

[60] J. Moolayil, *Learn Keras for Deep Neural Networks—A Fast-Track Approach to Modern Deep Learning With Python*, 2nd ed. New York, NY, USA: Springer, 2019.

[61] B. V. Babu and M. M. L. Jehan, "Differential evolution for multi-objective optimization," in *Proc. Congr. Evol. Comput., CEC*, vol. 4, Dec. 2003, pp. 2696–2703, doi: 10.1109/CEC.2003.1299429.

[62] S. S. Reddy and P. R. Bijwe, "Multi-objective optimal power flow using efficient evolutionary algorithm," *Int. J. Emerg. Electric Power Syst.*, vol. 18, no. 2, p. 233, Jul. 2017, doi: 10.1515/ijeeps-2016-0233.

[63] R. Storn and K. Price, "Differential evolution—A simple and efficient heuristic for global optimization over continuous spaces," *J. Global Optim.*, vol. 11, no. 4, pp. 341–359, 1997, doi: 10.1023/A:1008202821328.

[64] L. Li and Q. Liu, "Acceleration curve optimization for electric vehicle based on energy consumption and battery life," *Energy*, vol. 169, pp. 1039–1053, Feb. 2019, doi: 10.1016/j.energy.2018.12.065.

[65] S. S. Reddy, "Optimizing energy and demand response programs using multi-objective optimization," *Electr. Eng.*, vol. 99, no. 1, pp. 397–406, Mar. 2017, doi: 10.1007/s00202-016-0438-6.

[66] *Provincial Electricity Authority (PEA). Thailand*. Accessed: Apr. 1, 2020. [Online]. Available: https://www.pea.co.th/e

[67] *Thai Meteorological Department (TMD), Thailand*. Accessed: Apr. 1, 2020. [Online]. Available: https://www.tmd.go.th/en

[68] *Department of Alternative Energy Development and Efficiency, Ministry of Energy, Thailand*. Accessed: Apr. 1, 2020. [Online]. Available: http://weben.dede.go.th/webmax/

[69] (2020). *BiHiKu: Bifacial High Power Dual Cell PERC Module (Poly & Mono), Canadian Solar, Guelph, Ontario, Canada*. [Online]. Available: https://www.canadiansolar.com/bihiku/ (accessed on 1 May 2020).

[70] Edison Electric Institute. (Sep. 2019). *Electric Vehicle Sales?: Facts & Figures*. Washington, DC, USA. Accessed: May 1, 2020. [Online]. Available: https://www.eei.org/issuesandpolicy/electrictransportation/

[71] *Tesla Model 3*. Accessed: May 1, 2020. [Online]. Available: https://www.tesla.com/model3

[72] *Tesla Model S*. Accessed: May 1, 2020. [Online]. Available: https://www.tesla.com/model3

[73] *Chevy Volt Plug in Hybrid*. Accessed: May 1, 2020. [Online]. Available: https://www.chevrolet.com/electric/volt-plug-in-hybrid

[74] *Nissan Leaf*. Accessed: May 1, 2020. [Online]. Available: https://www.nissanusa.com/ vehicles/electric-cars/leaf/

[75] C. Choi, H. Noh, S. Kim, R. Kim, J. Lee, J. Heo, and H.-T. Kim, "Understanding the redox reaction mechanism of vanadium electrolytes in all-vanadium redox flow batteries," *J. Energy Storage*, vol. 21, pp. 321–327, Feb. 2019, doi: 10.1016/j.est.2018.11.002.

[76] IEA. *Average CO_2 Emissions Intensity of Hourly Electricity Supply in the European Union, 2018 and 2040 by Scenario and Average Electricity Demand in 2018, IEA, Paris*. Accessed: May 1, 2020. [Online]. Available: https://www.iea.org/data-and-statistics/charts/average-co2-emissions-intensity-of-hourly-electricity-supply-in-the-european-union-2018-and-2040-by-scenario-and-average-electricity-demand-in-2018

CHITCHAI SRITHAPON (Graduate Student Member, IEEE) received the B.Eng. degree in electrical engineering from Khon Kaen University, Khon Kaen, Thailand, in 2002, and the M.Eng. degree in mechatronics engineering from the Suranaree University of Technology, Nakhon Ratchasima, Thailand, in 2009. He is currently pursuing the Ph.D. degree with the Department of Electrical Engineering, Khon Kaen University. Since 2008, he has been an Electrical Engineer with the Provincial Electricity Authority (PEA), Thailand. His main research interests include smart microgrids, energy management systems, power system optimization, and machine learning.

PRADIT FUANGFOO received the B.Eng. degree (Hons.) in electrical engineering from Kasetsart University, Bangkok, Thailand, in 1993, the M.Eng. degree in electrical engineering from Chulalongkorn University, Bangkok, Thailand, in 1996, and the Ph.D. degree from The University of Texas at Arlington, Arlington, TX, USA, in 2006. He is currently an Assistant Governor with the Provincial Electricity Authority (PEA), Thailand. He has authored or coauthored many journal articles and conference papers in power engineering. His main research interests include power system analysis, power system reliability, power distribution planning, power system protection, power quality, and smart grid.

PRASANTA K. GHOSH (Life Senior Member, IEEE) is currently a Professor with the Department of Electrical Engineering and Computer Science, Syracuse University, Syracuse, NY, USA. He has been conducting research in the area of microelectronics and power engineering. He has authored and/or coauthored many journal articles and conference papers on thin films, solid-state devices, and power engineering. His current research interests include smart grid systems, microgrid design and analysis, renewable energy resources, and EVs.

APIRAT SIRITARATIWAT received the B.Eng. degree (Hons.) in electrical engineering from Khon Kaen University, Thailand, in 1992, and the Ph.D. degree from The University of Manchester, Manchester, U.K., in 1999. He is currently a Professor with the Department of Electrical Engineering, Khon Kaen University. He has done research in HDD. He is one of the Pioneer Researcher of ESD/EOS and EMI in recording heads. He has published more than 100 articles and holds four pending patents. His current research interests include electromagnetics, electric machine design, smart grid, and power system optimization.

RONGRIT CHATTHAWORN received the B.Eng. degree (Hons.) in electrical engineering from Khon Kaen University, Thailand, in 2009, and the M.Eng. degree in electrical engineering and the Ph.D. degree from Chulalongkorn University, Thailand, in 2011 and 2015, respectively. From 2015 to 2017, he was a Researcher with the Energy Regulatory Commission (ERC), Thailand. Since 2018, he has been an Assistant Professor with the Department of Electrical Engineering, Khon Kaen University. His research interests include power system planning, power system reliability, smart grid, energy management systems, and renewable energy resources.